2018

Kinetics and Ensemble Dynamics of Colloidal Ellipsoids near an AC Electrode

Jiarui Yan
Cleveland State University

KINETICS AND ENSEMBLE DYNAMICS OF COLLOIDAL ELLIPSOIDS NEAR AN AC ELECTRODE

JIARUI YAN

Bachelor of Engineering in Macromolecular Materials and Engineering

Harbin Institute of Technology

June 2014

Submitted in Partial Fulfillment of Requirements for the Degree

MASTER OF SCIENCE IN CHEMICAL ENGINEERING

at the

CLEVELAND STATE UNIVERSITY

August 2018

We hereby approve this thesis for

JIARUI YAN

Candidate for the Master of Science in Chemical Engineering degree for the

Department of Chemical and Biomedical Engineering

and the CLEVELAND STATE UNIVERSITY'S

College of Graduate Studies by

Thesis committee chairperson, Dr. Christopher Wirth
Department of Chemical and Biomedical Engineering
Cleveland State University

Date

Thesis committee member, Dr. Geyou Ao
Department of Chemical and Biomedical Engineering
Cleveland State University

Date

Thesis committee member, Dr. Shawn Ryan
Department of Mathematics
Cleveland State University

Date

Student's Date of Defense: August 9, 2018

DEDICATION

I dedicate this work to my parents, Mr. Xiaobao Yan and Mrs. Xiaomao Zeng, for all their support. Through their unconditional love, I shall find my path to the essence of science.

ACKNOWLEDGEMENTS

I would like to express my deep gratitude to Dr. Christopher L. Wirth, my research advisors, for his patient mentorship and enthusiastic encouragement throughout my time as a graduate student. His willingness to give his valuable time has been appreciated and I am blessed to be a part of the Wirth Lab. Thank you so much for all your support.

Special thanks should be given to Dr. Moo-Yeal Lee, Dr. Fodor Petru, and Mr. Miroslav Bogdanovski, who helped and guided me in operating plasma cleaner.

I want to express my sincere gratitude to my thesis committee members Dr. Geyou Ao and Dr. Shawn Ryan for their suggestions. Also, I would like to thank Dr. Joanne Belovich, Dr. Nolan Holland, Dr. Alejandro Serrano, Dr. Orhan Talu, Dr. Marvin Thrash, Ms. Becky Laird and Ms. Darlene Montgomery for helping me during the past two years. The financial support from the Department of Chemical and Biomedical Engineering, Cleveland State University, in the form of research and teaching assistant positions is acknowledged. Thanks to Washkewicz College of Engineering for the scholarship.

To my colleagues in the Wirth Lab – Aidin, Cornelius, Kenneth, Marissa, Marola, Mohammed, Naik, Selwin, and William in the department - Alexander, Blas, Chan, Dustin, Kara, SooYeon, and Venkat. It has been a pleasure getting to know you all.

At last, to my most understanding parents, Mr. Xiaobao Yan and Mrs. Xiaomao Zeng. I will not forget your sacrifice of love and I love you forever.

KINETICS AND ENSEMBLE DYNAMICS OF COLLOIDAL ELLIPSOIDS NEAR AN AC ELECTRODE

JIARUI YAN

ABSTRACT

The manipulation of colloidal particles via applying electric fields has been studied over the past 30 years due to the unique properties associated with the fabricated colloidal crystals. Most works in this field focused on utilizing an alternating current (AC) electric field with spherical particles. However, utilizing spherical colloidal particles as building blocks for complex microstructures has been challenging. Consequently, more recent work has shifted to employing complex colloids (anisotropic in nature) as building blocks for advanced materials. In our work, the phase diagram and the kinetics of assembling colloidal polystyrene ellipsoids under an AC electric field at low frequencies were studied. Specifically, the structure of colloidal ellipsoid ensembles under varying electric field potentials (0.5 V, 1.0 V, and 1.5 V) was measured at a periodically regulated frequency (30 Hz ~ 3000 Hz) and the same set of experiments was done for colloidal spheres as a comparable reference. Data suggested the approximate critical frequency for assembled particles depended on the aspect ratio and the inherent block anisotropy may impact the mesoscale structure. Additionally, the rate constant for the rapid aggregation of colloidal particles was calculated via the plot of singlet evolution at varying electric field conditions. Results showed an increase in applied potential and a larger aspect ratio for the colloidal ellipsoids both resulted in a larger rate constant.

TABLE OF CONTENTS

LIST OF TABLES

LIST OF FIGURES

CHAPTER I

INTRODUCTION

Assembly of nanometer to micrometer scale particles into structures of technological importance has been studied for the past three decades[1]. A variety of interactions, typically tuned with an external electric or magnetic field, will induce interactions that could be electromagnetic or hydrodynamic in nature. Early work focused on spherical particles with isotropic interactions that formed close-packed crystal structures. Although significant advances and technologies were developed with isotropic particles, recent work has transitioned to anisotropic nano- to micrometer scale particles.

Anisotropic particles can now be synthesized to have varying shape and surface chemistry[2]. Particles with variations in some property as a function of position along the surface will typically interact with neighboring particles in a separation and orientationally dependent fashion (as opposed to isotropic particles that only interact via separation dependent interactions). Consequently, anisotropic particles form more intricate structures that will interact with light in more sophisticated ways than close-packed crystals.

This thesis summarizes experimental work that measured the response of one class of geometrically anisotropic particles in response to an electric field. Experiments consisted of utilizing digital video microscopy to measure the response of ellipsoids of

varying aspect ratio very near an *AC* polarized electrode at different electric field conditions. The main intellectual contributions of this thesis are:

- Ellipsoids experience a hysteresis in the electric field mediated phase diagram in the region where particles "stand" on the electrode. Experiments showed the threshold for ellipsoidal particles to stand was different when ramping the electric field frequency up as compared to when ramping downward in frequency. Further, the size of the hysteresis regime scaled with the aspect ratio of the ellipsoids. The hypothesis for the physical mechanism for this behavior is that the rotational diffusion relaxes the particles' position following dipole alignment with the electric field; this relaxation depended on the particles' aspect ratio.
- The second intellectual contribution of this thesis was that the rate constant for short time aggregation depended on the shape of the ellipsoids. The scaled maximum aggregation rate for each type of particle was measured. Ellipsoids had a smaller maximum rate constant, which was consistent with the effect of aspect ratio on a generic Smoluchowski aggregation process.

CHAPTER II

LITERATURE REVIEW AND THEORY

2.1 Anisotropic particles

Preparing particles with functional patches is practically meaningful because the potential complex superstructures that could be obtained would lead the resulting materials to a different performance[2]. Typically, anisotropic particles that are involved in different research fields are rich in varieties, such as Janus particles, nanorods, and colloidal ellipsoids. There is more than one way to bring anisotropy into a particle, such as partially changing the physical or chemical properties of the surface of particles, making particles into different anisotropic shapes and applied these two methods at the same time. Based on that, lots of combinations could be carried out, which would result in various anisotropic particles (see **Figure 2.1**).

The most common two types could be categorized as chemically anisotropic particles and geometrically anisotropic particles.

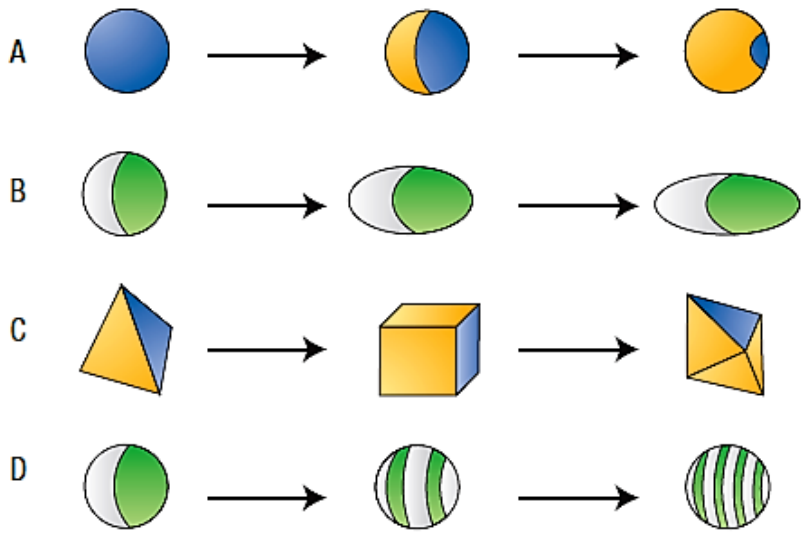

Figure 2.1: Series of anisotropic particles. A: Surface coverage, B: aspect ratio, C: faceting, D: surface pattern quantization.[2]

2.1.1 Chemically anisotropic particles

A particle with non-uniform surface chemical properties is considered a chemically anisotropic particle. One such chemically anisotropic particles is a "patchy" particle, where some portion of the native particle is covered with a second material. A Janus particle is when the patch covers approximately ~50% of the available surface area of the native particle. Thus, a Janus particle is one of the simplest chemically anisotropic particles, in particular, because although it is a chemically anisotropic particle, it has geometric isotropy.

For the fabrication of Janus particle, the most flexible way is masking technique, via which functional groups could be grafted on the surface of the targeting particles and some metal materials could be deposited as well. Usually, to fabricate an anisotropic particle, the surface of the particle is partially exposed so that the physical and/or chemical properties for that certain area would be modified after the grafting or deposition. There are two challenges that researchers are primarily dealing with: the controllability of the geometry (e.g. the relative areas of two half parts) and the productivity of the fabrication

in large quantities, which would be crucial to practical applications[3]. Until now, many proper methods have been developed for the synthesis of Janus particles. For instance, Chia-Hung C. *et al.* [4] have tried to prepare Janus particles via an immiscible fluids-based method that developed by themselves. The resulting particles are highly monodispersed and morphologically regulatable. Jiang S. *et al.*[5] introduced another decent method to form Janus particles with particle-stabilized emulsions (Pickering emulsions). The most outstanding part of this method is it has not only the controllability of the geometry for Janus particles in a wide size range but also the ability to synthesize particles in a relatively large quantity during the synthesis process. Also, in 2010, McConnell *et al.*[6] developed a new method for obtaining patchy gold-on-silica Janus particles with optical properties in multi-regions and they could be tunable via a self-assembly process.

As the surface coverage of Janus particles is approximately 50 %: 50 % distinct in chemistry, electrical, polarity, and other properties, Janus particles are suitable for application as anisotropic building switchable displays[7], and smart nanomaterials such as blocks for complex structures[2], optical sensors[6], biological sensors, nanomotors and antireflection coatings[8]. Smoukov *et al.*[9] reported the assembly of magnetic Janus particles that staggered chain structures could be created under the magnetic or electric fields and this magnetic assembly of particles could maintain the structure permanently, which could be taken apart as desired by demagnetization. This work makes the reversible and responsive selective assembly of magnetic particles become possible and applications in circuits or as sensors would be benefit from it as well.

To characterize chemically anisotropic particles, techniques like conventional Transmission electron microscopy (TEM), scanning electron microscope (SEM), Small-

angle X-ray scattering, and Two-dimensional nuclear over-hauser effect spectroscopy nuclear magnetic resonance spectroscopy (2D NOESY NMR) have been widely used to determine the exact structure of patchy, multi-compartment and Janus particles, but it is still difficult to completely reveal the structure of the particle's surface[10]. Most of the time, TEM is used to collect the factual information for the formation of the anisotropic particles.

2.1.2 Geometrically anisotropic particles

In a 3D system, particles could be considered as geometrically anisotropic particles when they are simply not spherical. Any non-spherical properties of their shape would introduce geometric anisotropy into particles. The reason why geometrically anisotropic particles got the attention from scientists is because particle shape plays a crucial role in assembly. The geometry can not only control the recognition of particles but also regulate the structure of colloidal particle packings and the distribution of bind surface charges. In a 2D micro-system, the structure that could be obtained from monodispersed spherical particles would be hexagonal only.

One way to bring geometric anisotropy into the system is utilizing colloidal spheres possess different diameters, which was reported by Ning Wu *et al*.[11]. Anisotropic clusters would form under AC electric field (see **Figure 2.2**). For anisotropic polystyrene (PS) dumbbell particles and colloidal ellipsoids, they are usually processed from a spherical particle and its surface area is greater the original sphere's. By adjusting the salt concentration and the frequency of the applied electric field, Ning Wu *et al.*[12] claimed that they are able to control both orientation and aggregation of colloidal dimers precisely.

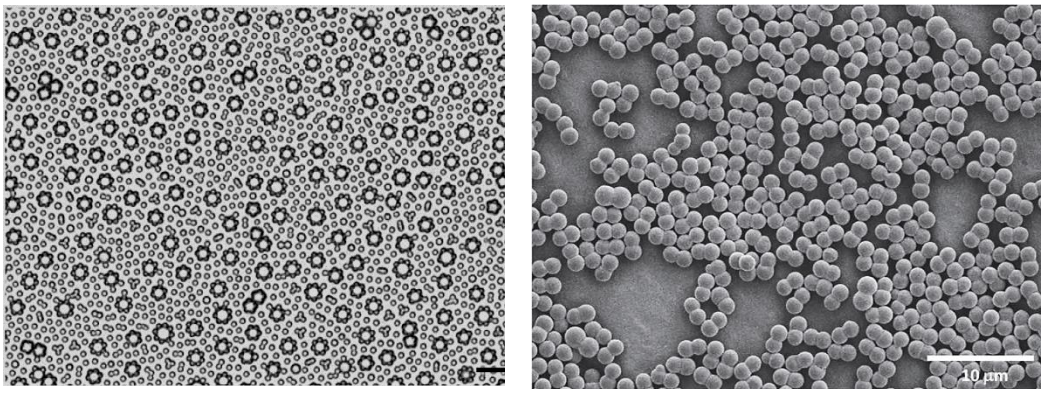

Figure 2.2: Binary colloidal spheres[11] (left) and colloidal dimers[12] (right).

To prepare dumbbell particles, Jin-Woong K. *et al.*[13] took advantage of the cross-linked PS and the seeded polymerization. Swelling and tumbling were performed as in the seeded cross-linked polystyrene synthesis, which resulted in a phase separation before the occurrence of polymerization. Ho *et al.*[14] provided a mechanical deformation method. They made PS latex dispersed in the poly (vinyl acetate) (PVA) water solution and cast films on a substrate. The PS spheres in the films could be stretched with the film when the glass transition temperature of PVA was reached. The final colloidal ellipsoids were collected from the stretched films by dissolving the films in alcoholic solutions. Moreover, with this ellipsoidal particle fabrication technique, the study from Vermant *et al.*[15] suggests the aspect ratio of geometrically anisotropic particles could affect the potential formation of liquid-crystalline as well as the configuration of clusters' microstructure via AC electric field.

To characterize geometrically anisotropic particles, the most common method is through optical video microscopy and SEM. SEM experiments could even reveal the part of the particles that were treated differently during the fabrication process[16].

2.2 Colloids interactions

2.2.1 Equilibrium and non-equilibrium dynamics in the z-direction

Consider the micrometer scale "colloidal" spheres as shown in **Figure 2.3**. The colloids have a radius *R* and separation distance from the nearby electrode *h*. The separation distance between the colloids is *D*.

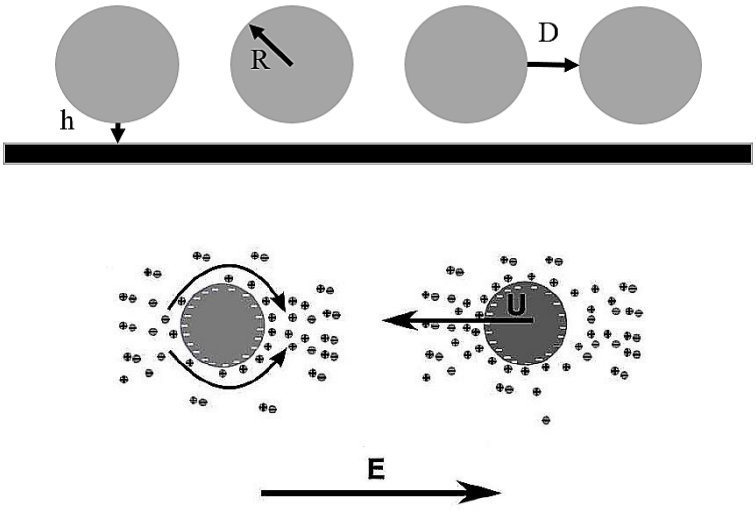

Figure 2.3: Colloidal spheres nearby the electrode.

A typical colloid has a strong bound surface charge. For instance, the experiments described herein use polystyrene particles with a bound sulfate negative charge. The surface charge of the colloidal particles and the addition of electrolytes would impact the stability of colloidal dispersions. The electrostatic interaction between the surrounding ions and the charged surface attracts repels co-ions and counterions from the charged surface. Thus, a layer that is the combination of the strong bound negative charge and the nearby excess of mobile cations and this layer is known as the electric double layer (EDL). It can be divided into two individual layers: the stern layer and diffuse layer. Within this diffuse layer is a notional boundary, known as the slipping plane. The potential at the boundary

that is caused by the behavior of a single particle within this boundary is called zeta potential.

In addition to the surface of the particle, the surface of the electrode has an electric double layer. The overlap of these two physiochemical structures induces repulsion that keeps the colloidal particles separated from the electrode and mobile during experiments. A colloidal particle will also experience gravity if the density of the particle does not match that of the fluid. Finally, there may also be a strong Van der Waals interaction between the particle and nearby substrate. The superposition of these three forces is given by[17]:

$$F_c(h) = -\frac{d\Phi_c}{dh} = \kappa B \exp(-\kappa h) - 6.8\lambda kT \exp(-\lambda h) - G \quad (1)$$

Where $F_c(h)$ is the height dependent force, equal to the negative derivative of the interaction energy $-\frac{d\Phi_c}{dh}$, κ is the Debye parameter, B is the interaction parameter that depends on the particle and electrode properties, h is the separation distance, λ is the characteristic decay length of the Van der Waals attraction, k is Boltzmann's constant, T is temperature, and G is the net weight of the particle.

Upon application of the electric field, the mobile charge associated with the particle and electrode surface responds such that electroosmotic flow fields are driven in the plane tangent to either surface. Electroosmosis usually occurs when there are flows of fluid going through the charged channel under a longitudinal electric field, due to the formation of a thin double layer that caused by a cloud of mobile counterions, which is attracted by the charged channel wall. The presence of an external field would force the excess free ions within the Debye layer move. Meanwhile, these ions would carry fluid with them lead (see **Figure 2.4**). The fluid movement can be further extended to the bulk of the channel through the effect of viscous stress. The same mechanism also causes the translation of a charged

particle under an electric field, i.e., electrophoresis (see **Figure 2.4**). Both electroosmosis and electrophoresis were first observed by Reuss and he discovered water flow as well as the motion of charged clay particles through a bed of quartz sand[18].

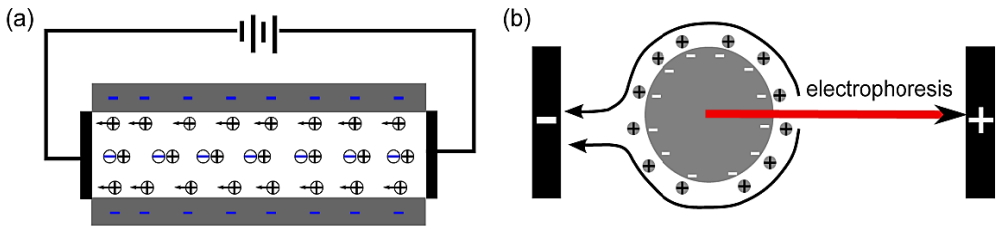

Figure 2.4: (a) Electroosmosis in a negatively charged channel. (b) Schematic of a negatively charged particle's electrophoresis under uniform electric fields.[19]

For the situation considered herein, the electroosmotic flow fields will induce motion normal to the surface of the electrode that has been both predicted and observed experimentally[20]. These motions could be explained by Bernoulli's principle. For aggregation, since the electroosmotic flow around a particle has a certain direction, the velocity of the flow between two neighboring particles could increase if their flow directions agree with each other synchronously. According to the Bernoulli's principle, that would result in a reduction of pressure in the space between them and a corresponding pressure gradient occurs subsequently, which is the driving force of creating a favorable environment for assembly. Also, building a 2D electroosmotic streamline model for particles in the *xy*-plane could give us a better understanding of the aggregation mechanism (see **Figure 2.5**). In other words, the resultant velocity of surface electroosmotic flow between particles determines their relative motions. These studies have shown that particles respond with both steady and oscillatory modes in the *z*-axis, both of which will profoundly impact the lateral motion of particles in the *xy*-plane.

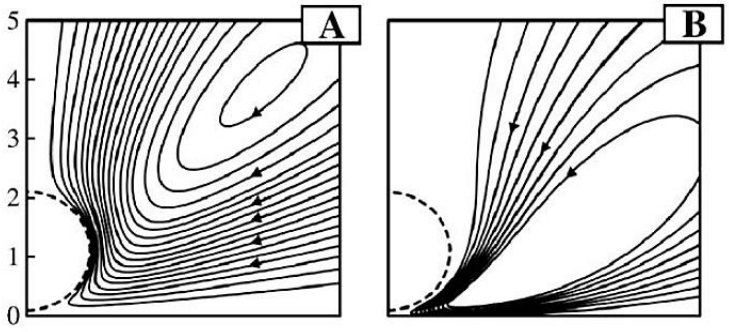

Figure 2.5: The streamlines of electroosmotic flow generated by the action of the electric field action on the equilibrium diffuse clouds of the particle (ζp) and/or the electrode (ζe). (a). ζp=−100 mV, ζe=0 and (b) ζp=0 and ζe=−100 mV.[20]

2.2.2 Colloidal dynamics in the xy-plane in the presence and absence of an electric field

This thesis is concerned with the response of a psudeo-2D layer of colloidal spheroids very near an electrode surface. The response measured experimentally described later in the thesis is a consequence of equilibrium dynamics and those associated with the application of an electric field. In the absence of an electric field, particles undergo random Brownian fluctuations that induce the ensemble to assume a random spatial distribution at the surface concentrations concerned with herein. Higher surface concentrations will induce particle organization into solid-like crystalline phases[21]. Particles will also interact via equilibrium surface interactions, similar to those described by Equation (1), that will induce slight variations in the microstructure. An example of an ensemble of both colloidal spheres and ellipsoids in the absence of an electric field is shown in **Figure 2.6**.

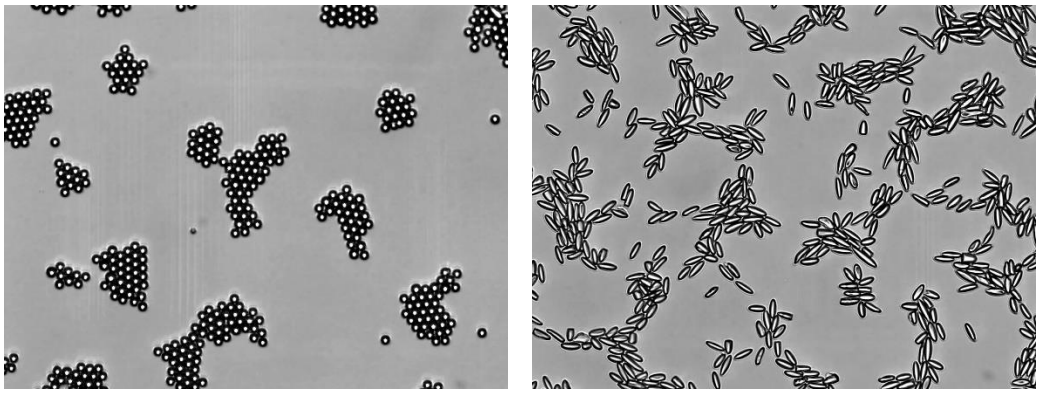

Figure 2.6: Clusters of colloidal spheres (left) and ellipsoids (right) formed under the AC electric field.

In response to an electric field, electroosmotic flow fields will be induced along then particle and electrode surfaces. As described above, these flow fields will induce a force felt by individual particles. However, electric field induced flow fields will also cause local attraction or repulsion depending on various experimental parameters. Consider the "target" particle shown in **Figure 2.7**. The target particle has electroosmotic flow fields associated with it that will induce neighboring particles to either be attracted or repelled. For steady, or DC, electric fields, the sign of the electric field and the particles' surface charge dictate whether the net force is repulsive or attractive. When the electric field is positive and the diffuse cloud of the electric double layer has an excess of cations (as would be the case for a particle with bound negative charge), the flow field rotates clockwise to attract neighboring particles. Reversing the sign of the steady electric field or the sign of the charge associated with the particles will reverse the net sign of the force.

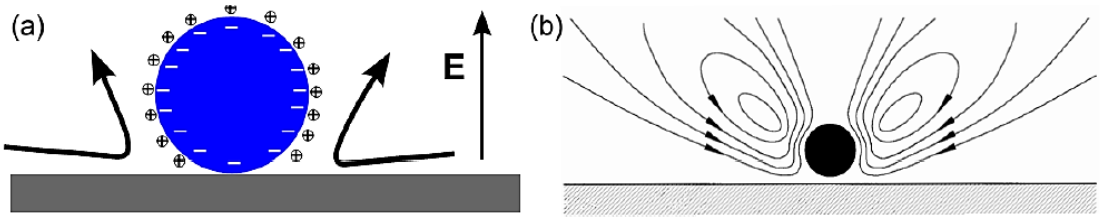

Figure 2.7: (a) Schematics of a negatively charged colloidal sphere nearby the electrode that surrounded by the ECEO flow. (b) the theoretical streamlines for ECEO flow.[19, 22]

As described above, the problem becomes more difficult, however, when considering the response of a particle to an AC electric field. The flow field generated along the particle surface is no longer steady but instead oscillates at the frequency of the applied electric field. For example, the flow field generated along the particle surface oscillates at the frequency of the applied electric field. In addition, the particle experiences small amplitude oscillations in height in response to the AC electric field (see **Figure 2.8**). The combination of these two modes of motion, the oscillatory flow field, and oscillations in height, cause either aggregation or separation of particle pairs. The sign of the interparticle force depends on the break in symmetry between the two oscillatory modes of motion. The key to predicting whether particles exposed to an AC electric field will aggregate or separate is in the phase angle between the two oscillatory modes of motion. Particles will separate if the phase angle between the oscillations in the electric field and particle height is $< 90^{\circ}$, but particles will aggregate if the phase angle is $> 90^{\circ}$.

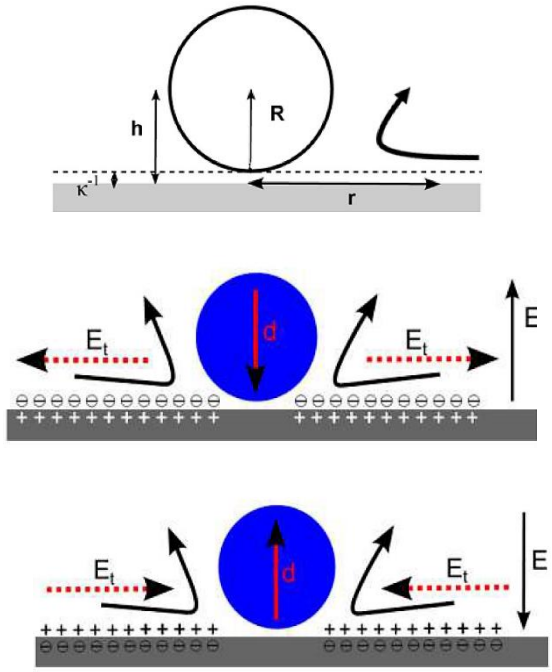

Figure 2.8: The sphere is nearby the electrode, where its distance from the electrode *h*, the Debye length κ^{-1} is much smaller than the radius *R*.[19, 23]

There is yet another mechanism by which particles can aggregate/separate that depends upon the charge induced along the electrode surface[23]. An electrode will induce accumulation of charge as a consequence of polarization but in the absence of faradaic (i.e. reaction mediated) charge transfer. Net accumulation of charge will be positive when the electrode had a negative polarization and negative when the electrode has a positive polarization. Further, electric field components from this polarization will act on this induced charge to produce flow. The combination of these effects, broadly termed induced charge electroosmosis (ICEO), means that the mechanism has a rectified component even during oscillatory polarization. The rectified component flow field scales inversely with the frequency ($\sim f^{-1}$) but scales with the square of the electric field ($\sim E^2$). Thus, many authors have attributed the steady response of particles to oscillatory fields as a consequence of the

ICEO mechanism because of some salient features of experiments that appear to agree with ICEO.

2.2.3 Colloidal aggregation

As described above, particles will tend to either aggregate or separate resulting from a net force experienced by individual particles. There are a variety of ways in which this structural evolution may be tracked, including tracking average nearest neighbor distance, average cluster size, pair distance at infinite dilution, and pair distribution function. In the work described herein, the aggregation process was tracked with the classic Smoluchowski analysis typically employed for tracking flocculation in bulk systems. This analysis was also used once previously to track the response of spheres to an applied AC electric field.[24]

Consider the ensemble of particles in a single plane shown in **Figure 2.5**. When only considering singlet lost to clusters without cluster breakup, the singlet loss rate is given by:

$$\frac{dn_1}{dt} = -k_e n_1^2 \tag{2}$$

Where n_1 is the number of singlets and k_e is the rate constant in units of area/time. Following the integration of Equation 2 and defining $n_1(t = 0) = n_{1,0}$:

$$\frac{n_{1,0}}{n_1} = 1 + k_e n_1 t \tag{3}$$

Equation 3 is of utility in the experiments described below where singlet concentration can be directly measured. Rearranging Equation 3 such that the product of k_e and t are isolated:

$$\frac{1}{n_{1,0}} - \frac{1}{n_1} = k_e t \tag{4}$$

Thus, plotting the left-hand side of Equation 4 versus time should give a straight line with slope equal to the rate constant, k_e.

As described previously, the rate constant is expected to depend on the electric field conditions[24]. A particulate system aggregating strongly at a given set of electric field conditions will have a larger rate constant when compared to a system aggregating less strongly at a different set of conditions. Previous work had shown that spheres have a rate constant that depended on the square of the electric field strength and on the inverse of the frequency[11, 17, 20–25]. However, there has been no work elucidating the impact of shape on the rate constant for colloids responding to a nearby polarized electrode.

2.2.4 **Brownian motion**

In a typical solution, the size of ellipsoids ranges from a few nanometers to several micrometers, where Brownian motion plays a decisive role. Brownian motion induces the ellipsoids suspended in the fluid to move randomly and the mean squared displacement is the most common method of calculating the spatial extent of this kind of random motion. In general, MSD measures the square of the distance between the reference position and the targeting particle's position in the deviation time (lag time). The main purposes of analyzing MSD is to obtain the diffusion coefficient value D and to determine what type of diffusion regime the ellipsoids are undergoing. The equation for determining two-dimensional (2D) translational MSD here can be written as:

$$MSD = v^2\Delta t + 4D_e\Delta t \tag{5}$$

where v and D_e are the propulsion speed and the effective diffusion coefficient of the ellipsoids. The effective diffusion coefficient is related to the apparent velocity of dispersed particles, which corresponds to the viscosity of bulk.

Dealing with 2D instead of 3D is one way to simplify the imaging processes as well as to get access to the collectible data and experimental requirements easier[26]. By Einstein's equation, the mean squared displacement can be used to calculate the diffusion coefficient[27]:

$$D_\theta = k_B T \,/\, \gamma_\theta \tag{6}$$

where k_B is the Boltzmann constant, T is the temperature and γ is the drag coefficient.

Because of the rotational motion that caused by the geometric asymmetry, analyzing the Brownian motion of ellipsoids is consider as a more challenging task when compared to the analysis of spheres[29]. Being affected by multiple forces, the ellipsoids will try to align along one of its axes so that the interaction energy would reach the minimum and for the short axis the rotational diffusion coefficient of colloidal ellipsoids, in theory, could be calculated via:

$$\gamma_\theta = 6\eta V G_\theta \tag{6}$$

$$G_\theta = \frac{2}{3}\frac{(p^4-1)}{p}\left[\frac{2p^2-1}{\sqrt{p^2-1}}\ln\left(p+\sqrt{p^2-1}\right)-p\right]^{-1} \tag{7}$$

where η is the fluid viscosity, $p = {}^{a}/_{b}$ is the aspect ratio, V is the volume, G is the geometric factor that characterizes the deviation of the ellipsoid from a sphere.[26]

CHAPTER III

EXPERIMENTAL PROCEDURE

3.1 Ellipsoids fabrication

We chose polystyrene (PS) as the materials for the particles that were used in our experiments, due to the fact that utilizing PS to obtain ellipsoidal particles is well developed[13]. The method we used for obtaining the colloidal ellipsoids is initially developed by Ho *et al.*[14].

First, we cleaned two 500 ml glass bottles with 80% of distilled water and 20% of ethanol in an ultrasonic bath for about 30 minutes. Then, bottles were rinsed with ultrapure water and kept uncapped in an oven to dry completely (make sure no ethanol resides). Afterward, the bottles were cooled down to room temperature by taking them out. 300 g of mQ-water was added in one of the dried bottles and bubbles should be got rid of before adding any PVA (Polyvinyl Alcohol). The magnetic stirrer was cleaned with 80% of distilled water and 20% ethanol and then dried before dropping into the solution. The bottle was placed on magnetic stirrer of steady rate 400 rpm and 7.5 g of Polyvinyl Alcohol (POVAL 40-88 Kuraray polyvinyl alcohol) was added bit by bit so that the formation of PVA lumps in the solution could be avoided. The solution was stirred for about 24 hours

and then filtered into the other 500 ml bottle (shown in **Figure 3.1**). Next, the filtered solution could be relaxed for about one hour to minimize the bubbles in the solution and then 1g (desired) of 6μm Polystyrene Sulfate latex particles (4% w/v) was added. Swirling the bottle gently with hand to ensure Polystyrene particles were dispersed uniformly in the PVA solution.

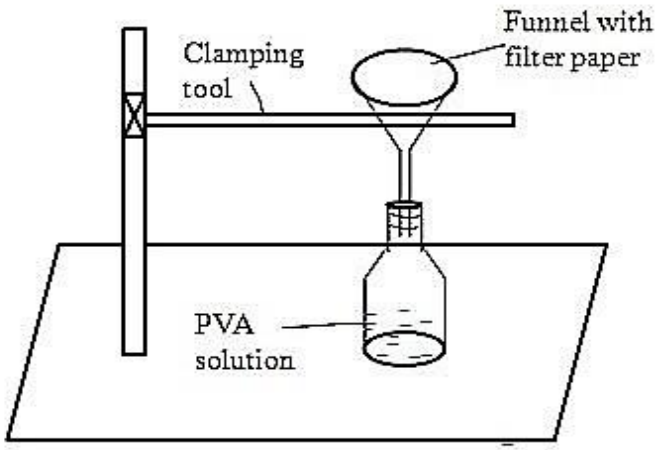

Figure 3.1: Preparation of filtrated PVA solution[30].

A 32 cm × 32 cm square boundary was constructed on a mirror tray by using caulk as shown in the (**Figure 3.2 (a)**). Thereafter, the mirror was cleaned multiple times in a sequence of acetone, ethanol, and mQ-water until a peeping sound was heard. It was made sure that no residues were left on the mirror tray after the clean procedure. Four sides of the mirror tray were leveled carefully by adjusting leveler screws with a leveler instrument, which could result in a finished film with a uniform thickness. Then, the solution was poured at the center of the square until it spreads to all four corners. The bubbles were pushed to the edges with a clean spatula. The casted film was left to dry for about two days

and then detached from the mirror carefully from the edges using the knife as shown in the **(Figure 3.2 (c)**).

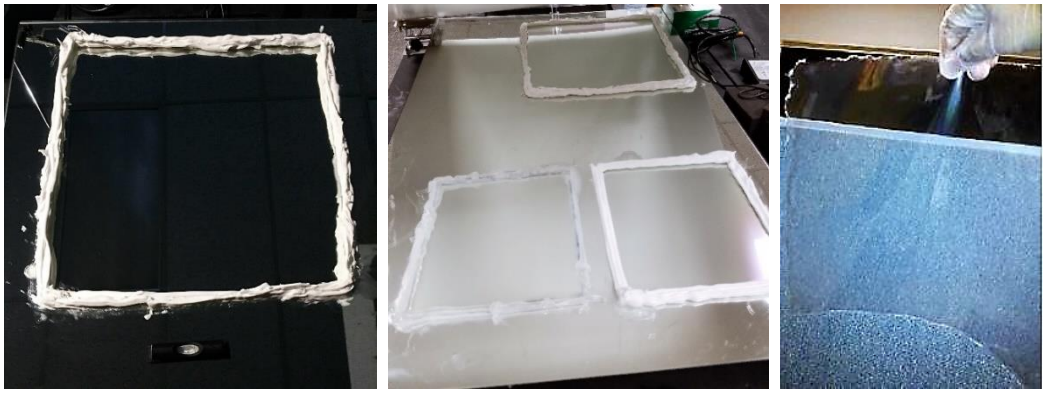

(a) (b) (c)

Figure 3.2: (a) Balanced mirror tray; (b) Filled with final PVA & PS mixture; (c) Peeing dried film off mirror tray.

The PVA film was cut into a size of 3×7cm by leaving half centimeter each on top and bottom and the grids of 1×1cm each were drawn to measure the final stretch. A set of metal blades were used to sandwich the film tightly by tuning the nuts and screws. The oven was preheated for about one hour before inserting the experimental setup for film stretching. Also, a supporting platform placed under the experimental set (as shown in **Figure 3.3**), which was designed to control the degree of stretching by regulating the height so that colloidal ellipsoids with different aspect ratios could be obtained eventually.

Figure 3.3: A piece of heated film landed on a supporting platform after its self-stretch.

Same middle section of stretched films was cut out and dissolved by a 3:7 mixture of isopropyl alcohol and mQ-water in a cleaned beaker. The resulting solution was then allowed to stir for 12 hours and then centrifuged and washed with the same IPA and water mixture for 3 more times. In the end, the particles were further centrifuged and washed with only mQ-water for 7 times before dispersing them in the KCl solution with a concentration of 10^{-6} M.

3.2 Assembly of parallel plate electrode fluid cell

The experimental setup consisted of a parallel plate electrochemical fluid cell. The fluid cell was assembled by sandwiching fluid between two electrodes as shown in **Figure 3.4**. The electrodes were two indium tin oxide coated glass sliders (with a surface resistivity of 30−60 Ω/sq, purchased from Sigma Aldrich). Silver conductive epoxy adhesives were used to attach the conducting wire on the ITO sliders. The sliders were sonicated in acetone and IPA for about 10 mins each. Then, they were further exposed to plasma oxygen in a plasma cleaner for another 10 mins, which could increase the number of negative surface charges. Note the way that we tried to clean the sliders before using was suggested by Ning

Wu[31]. One spacer (Secure seal spacer, eight wells, 9 mm diameter, 0.12 mm deep, molecular probes, life technologies) was placed on the conducting side of one slider and about 11 μL of the colloidal suspension was introduced onto the wells that provided by the spacer and was then sealed by the other ITO slider.

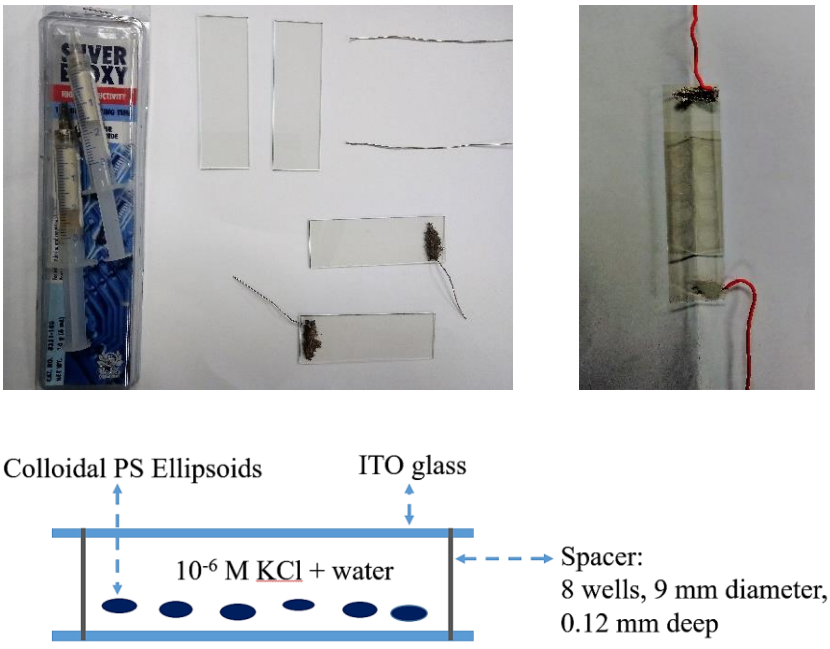

Figure 3.4: Assembling components for the experimental setup and the schematic section view of one fluid cells.

The fluid cell was carefully fixed on a stage holder and then placed on the microscope (Fixed Stage Upright Microscope System (Olympus BX51W1) with Hamamatsu ORCA-R2 digital deep-cooled CCD camera (C10600) from Olympus Microscopy through B&B Microscopy Limited.). The stage holder was further securely fixed onto the platform of the microscope with adhesive tape to avoid needless movement during the experiment. Two attached conducting wires were connected to a potentiostat (Reference 600+ 27 Potentiostat/Galvanostat/ZRA, obtained from Gamry Instruments) (**see Figure 3.4**) to introduce a tunable electric field between the ITO sliders. Also, the

isolation layer from conducting wires should be stripped off due to the later treatment would involve plasma cleaner.

Figure 3.5: The picture of the serviced microscope and potentiostat for the experiments.

3.3 Video filming and analysis

To determinate the phase diagrams of particles motion under different conditions, the process of filming videos with a microscope was operated by the software "cellSens Dimension". The 40× objective was chosen, the frame rate was set to 8 frames per second and the exposure time was fixed at 10 ms. Meanwhile, the length of each video was fixed at 60 min due to the limitation of the software and the applied frequency was regulated every 4 min so that there were 15 conditions varying over time throughout one complete video. Frequency and voltage are the only tunable parameters for the applied external electric field. Here, there were three different voltage (0.5 V, 1.0 V, and 1.5V) were used and each voltage was fixed for varying frequency. Specifically, for one set of videos that applied with the same voltage, the strategy of regulating frequency is raising it from 0 Hz

to 3000 Hz step by step and then bring it down back to 0 Hz. Once the filming is finished, we save the file as an AVI video.

To begin with, videos were duplicated and processed into binary (see **Figure 3.6.a – e**) and the subsequent holes that showed up in the videos were all be filled so that under a light background, a single particle would become a solid black spot and ImageJ would be able to recognize it properly. In order to quantitatively distinguish those particles with different aspect ratios, characterizations were performed and categorized for experiments. From the targeting video, we extracted a single frame (see **Figure 3.6.f**) in which majority of particles are separated from each other and run the "Analyze Particles" to obtain the average pixel size of particles directly from the result. Then, on the basis of this value, we chose the "Show: Bare Outlines" option and set a particle size range to run "Analyze Particles" again (see **Figure 3.6. g, h**) to screen out undesired particle clusters, which means after filling holes for the new generated bare outline image, we could obtain a binary image that only has singlet inside. Afterward, the global scale within ImageJ should be properly adjusted based on the magnitude of objective that was used and select measurements that are needed for the final "Analyze Particles" running. All the crucial date, such as the average size and the total number of particles would be generated into an excel spreadsheet during the entire process.

As for the further study of the relationship between particles motion and their geometric properties, a new series of video are necessary. We went through with the 20× objective to fit more particles into the visual field. Therefore, comparing with videos that were taken under 40× objective, the results could reveal the actual situation more precisely as a consequence of taking more research objects into account. The rest of software

configurations remain the same, but the length for an individual video became 2 min here, which consists of the initial 0.5 min without an electric field and the final 1.5 min with an electric field applied. As noted above, the electric field should be introduced immediately when the first quarter of a complete video ends.

Also, the method for analyzing this series of videos is slightly different from the previous one, since the record for a number of singlets in each frame is what we desired rather than the number of objects. Once videos are processed with the same method that we mentioned above, instead of analyzing video directly, the estimation of the average pixel size of particles should be accomplished first. First, we randomly extract one frame from the video, and crop an area contains several completely separated particles. Second, by analyzing that specific area of the picked frame, the average pixel size of particles would be obtained. Finally, set the boundary condition of size for the video analysis to screen out non-singlet objects from the video and this is the key point of tracking the fluctuation of singlet number. ImageJ could do the repetitive analysis via the build-in Marco program. (see **Appendix 1**)

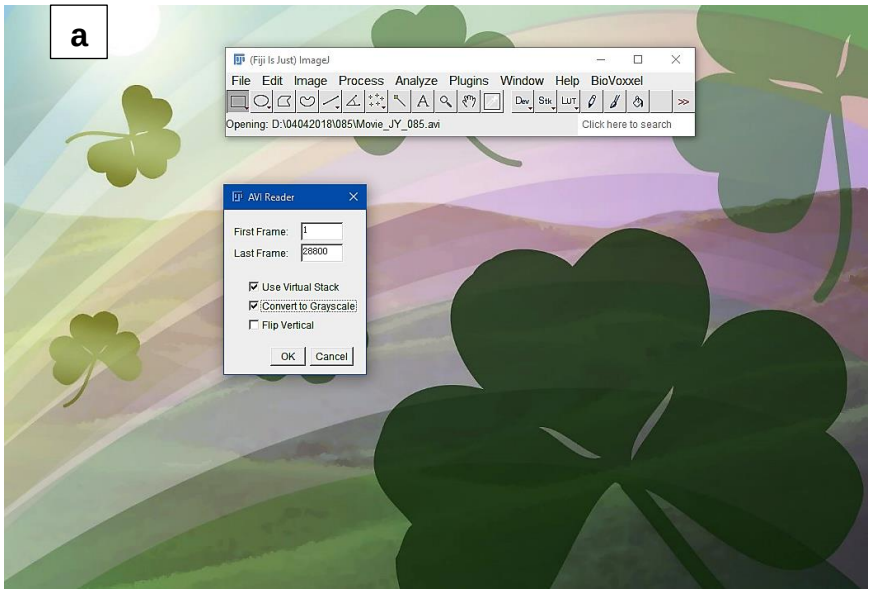

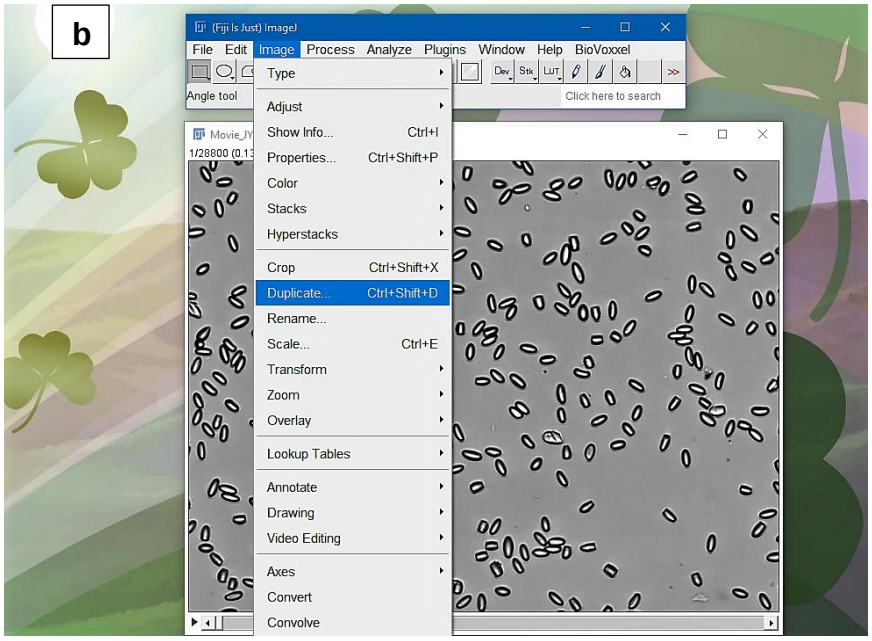
b
(Fiji Is Just) ImageJ
File Edit Image Process Analyze Plugins Window Help BioVoxxel
Angle tool
Click here to search
Type
Adjust
Show Info... Ctrl+I
Properties... Ctrl+Shift+P
Color
Stacks
Hyperstacks
Crop Ctrl+Shift+X
Duplicate... Ctrl+Shift+D
Rename...
Scale... Ctrl+E
Transform
Zoom
Overlay
Lookup Tables
Annotate
Drawing
Video Editing
Axes
Convert
Convolve

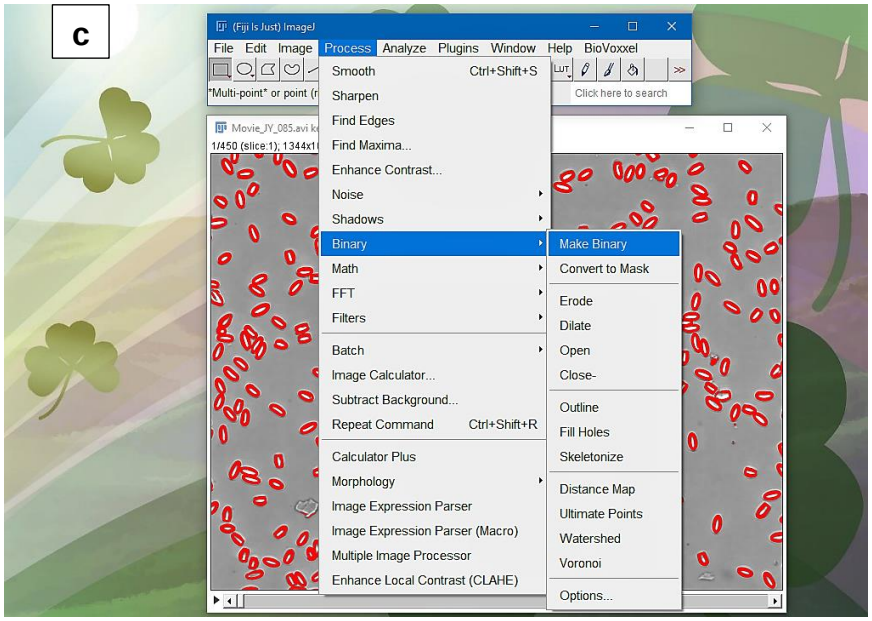
c
(Fiji Is Just) ImageJ
File Edit Image Process Analyze Plugins Window Help BioVoxxel
Click here to search
Smooth Ctrl+Shift+S
Sharpen
Find Edges
Find Maxima...
Enhance Contrast...
Noise
Shadows
Binary
Math
FFT
Filters
Batch
Image Calculator...
Subtract Background...
Repeat Command Ctrl+Shift+R
Calculator Plus
Morphology
Image Expression Parser
Image Expression Parser (Macro)
Multiple Image Processor
Enhance Local Contrast (CLAHE)
Make Binary
Convert to Mask
Erode
Dilate
Open
Close-
Outline
Fill Holes
Skeletonize
Distance Map
Ultimate Points
Watershed
Voronoi
Options...

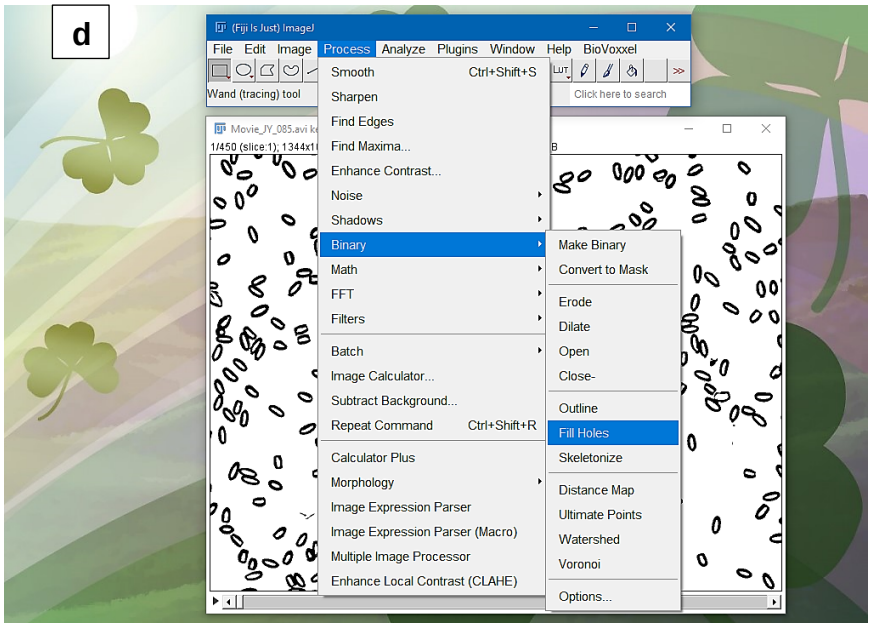
d
(Fiji Is Just) ImageJ
File Edit Image Process Analyze Plugins Window Help BioVoxxel
Wand (tracing) tool
Click here to search
Smooth Ctrl+Shift+S
Sharpen
Find Edges
Find Maxima...
Enhance Contrast...
Noise
Shadows
Binary
Math
FFT
Filters
Batch
Image Calculator...
Subtract Background...
Repeat Command Ctrl+Shift+R
Calculator Plus
Morphology
Image Expression Parser
Image Expression Parser (Macro)
Multiple Image Processor
Enhance Local Contrast (CLAHE)
Make Binary
Convert to Mask
Erode
Dilate
Open
Close-
Outline
Fill Holes
Skeletonize
Distance Map
Ultimate Points
Watershed
Voronoi
Options...

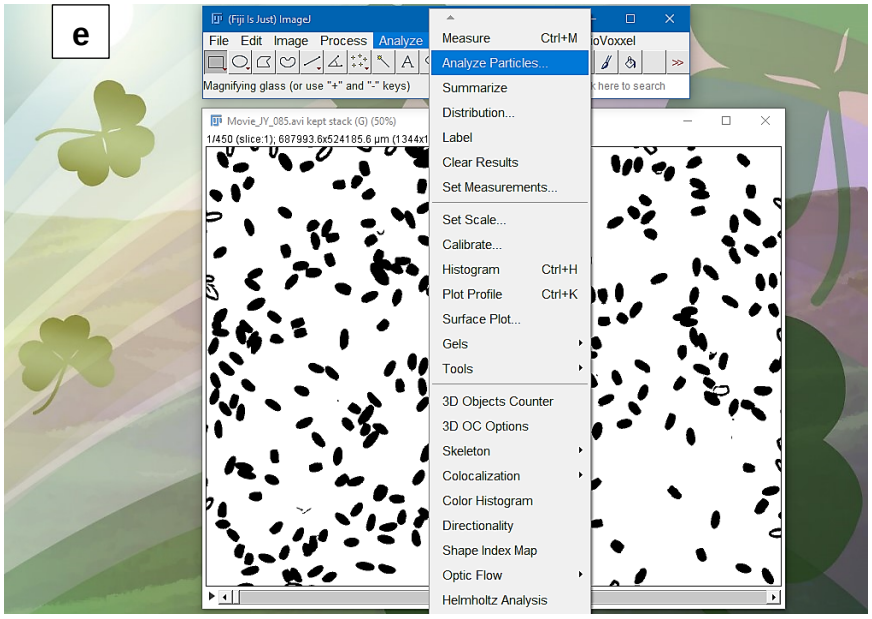
e
(Fiji Is Just) ImageJ
File Edit Image Process Analyze
Magnifying glass (or use "+" and "-" keys)
Measure Ctrl+M
Analyze Particles...
Summarize
Distribution...
Label
Clear Results
Set Measurements...
Set Scale...
Calibrate...
Histogram Ctrl+H
Plot Profile Ctrl+K
Surface Plot...
Gels
Tools
3D Objects Counter
3D OC Options
Skeleton
Colocalization
Color Histogram
Directionality
Shape Index Map
Optic Flow
Helmholtz Analysis

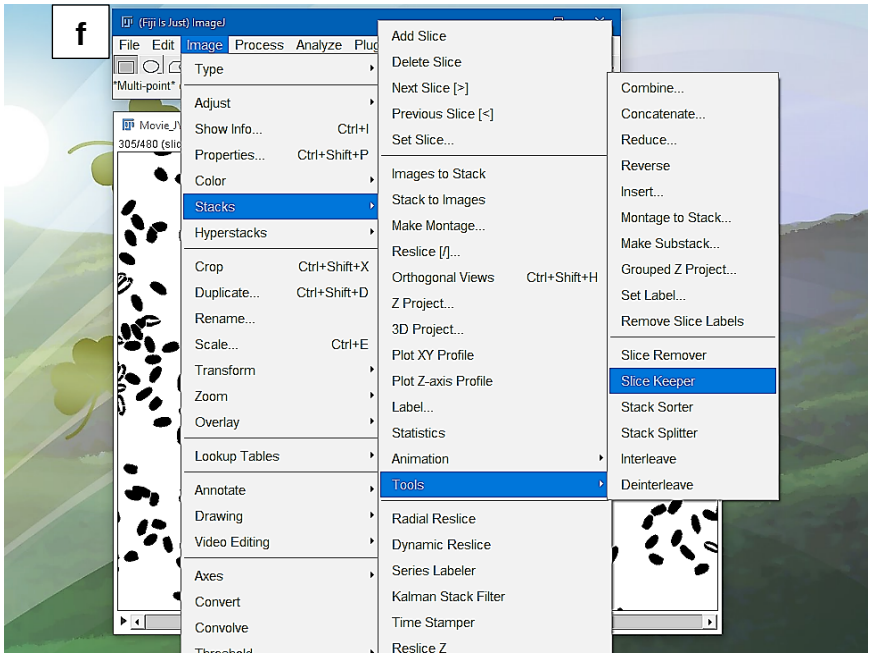
f
(Fiji Is Just) ImageJ
File Edit Image Process Analyze Plug
Type
Adjust
Show Info... Ctrl+I
Properties... Ctrl+Shift+P
Color
Stacks
Hyperstacks
Crop Ctrl+Shift+X
Duplicate... Ctrl+Shift+D
Rename...
Scale... Ctrl+E
Transform
Zoom
Overlay
Lookup Tables
Annotate
Drawing
Video Editing
Axes
Convert
Convolve
Add Slice
Delete Slice
Next Slice [>]
Previous Slice [<]
Set Slice...
Images to Stack
Stack to Images
Make Montage...
Reslice [/]...
Orthogonal Views Ctrl+Shift+H
Z Project...
3D Project...
Plot XY Profile
Plot Z-axis Profile
Label...
Statistics
Animation
Tools
Radial Reslice
Dynamic Reslice
Series Labeler
Kalman Stack Filter
Time Stamper
Reslice Z
Combine...
Concatenate...
Reduce...
Reverse
Insert...
Montage to Stack...
Make Substack...
Grouped Z Project...
Set Label...
Remove Slice Labels
Slice Remover
Slice Keeper
Stack Sorter
Stack Splitter
Interleave
Deinterleave

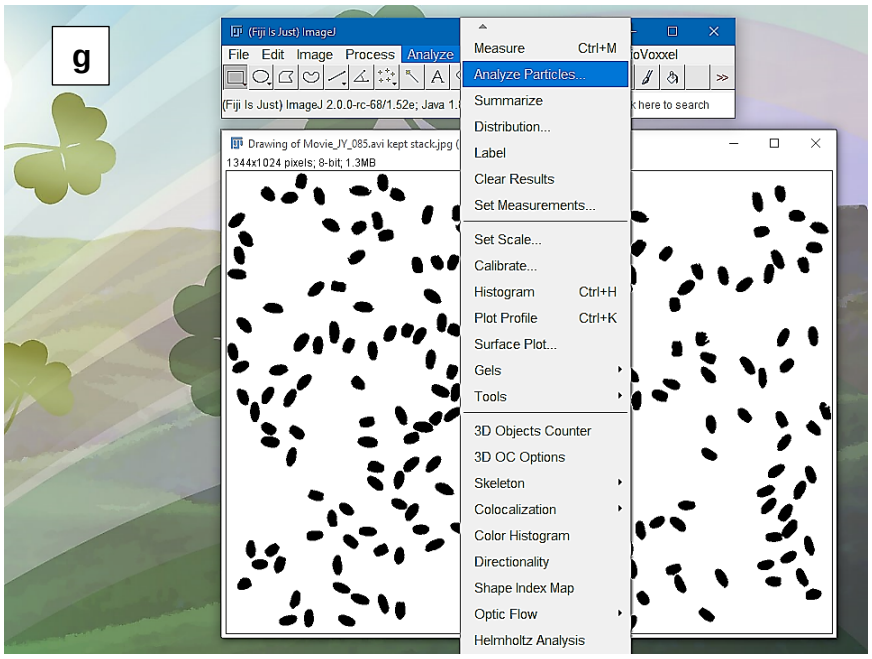
g
(Fiji Is Just) ImageJ
File Edit Image Process Analyze
Measure Ctrl+M
Analyze Particles...
Summarize
Distribution...
Label
Clear Results
Set Measurements...
Set Scale...
Calibrate...
Histogram Ctrl+H
Plot Profile Ctrl+K
Surface Plot...
Gels
Tools
3D Objects Counter
3D OC Options
Skeleton
Colocalization
Color Histogram
Directionality
Shape Index Map
Optic Flow
Helmholtz Analysis
Drawing of Movie_JY_085.avi kept stack.jpg
1344x1024 pixels; 8-bit; 1.3MB

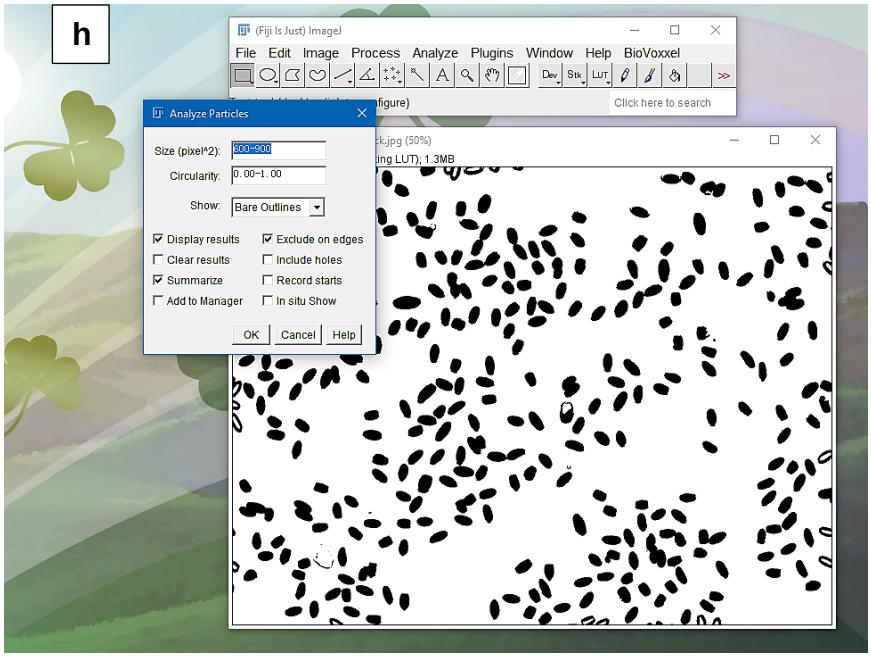
h
(Fiji Is Just) ImageJ
File Edit Image Process Analyze Plugins Window Help BioVoxxel
Click here to search
Analyze Particles
Size (pixel^2): 300-900
Circularity: 0.00-1.00
Show: Bare Outlines
Display results
Exclude on edges
Clear results
Include holes
Summarize
Record starts
Add to Manager
In situ Show
OK
Cancel
Help

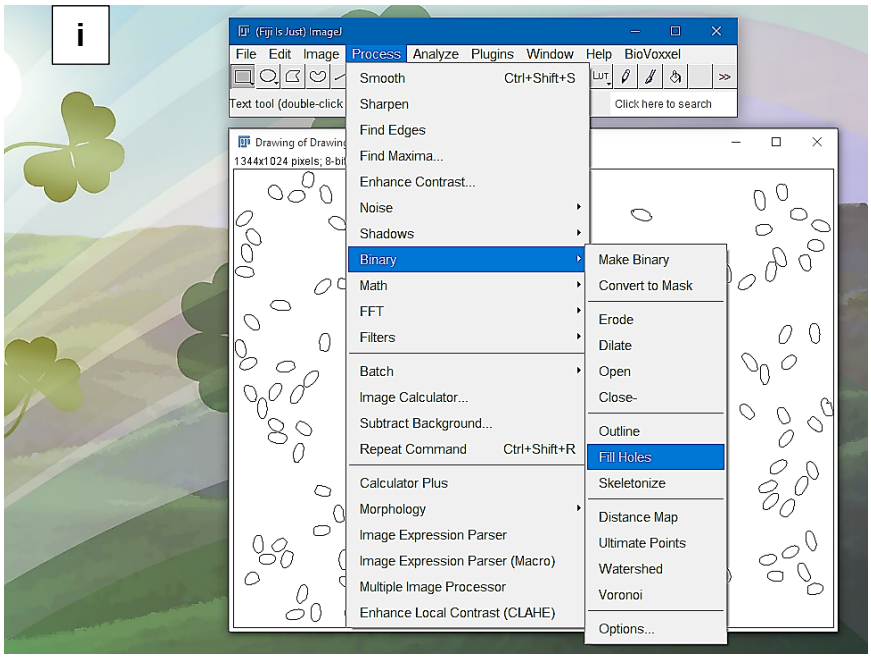
i
(Fiji Is Just) ImageJ
File Edit Image Process Analyze Plugins Window Help BioVoxxel
Click here to search
Smooth Ctrl+Shift+S
Sharpen
Find Edges
Find Maxima...
Enhance Contrast...
Noise
Shadows
Binary
Math
FFT
Filters
Batch
Image Calculator...
Subtract Background...
Repeat Command Ctrl+Shift+R
Calculator Plus
Morphology
Image Expression Parser
Image Expression Parser (Macro)
Multiple Image Processor
Enhance Local Contrast (CLAHE)
Make Binary
Convert to Mask
Erode
Dilate
Open
Close-
Outline
Fill Holes
Skeletonize
Distance Map
Ultimate Points
Watershed
Voronoi
Options...

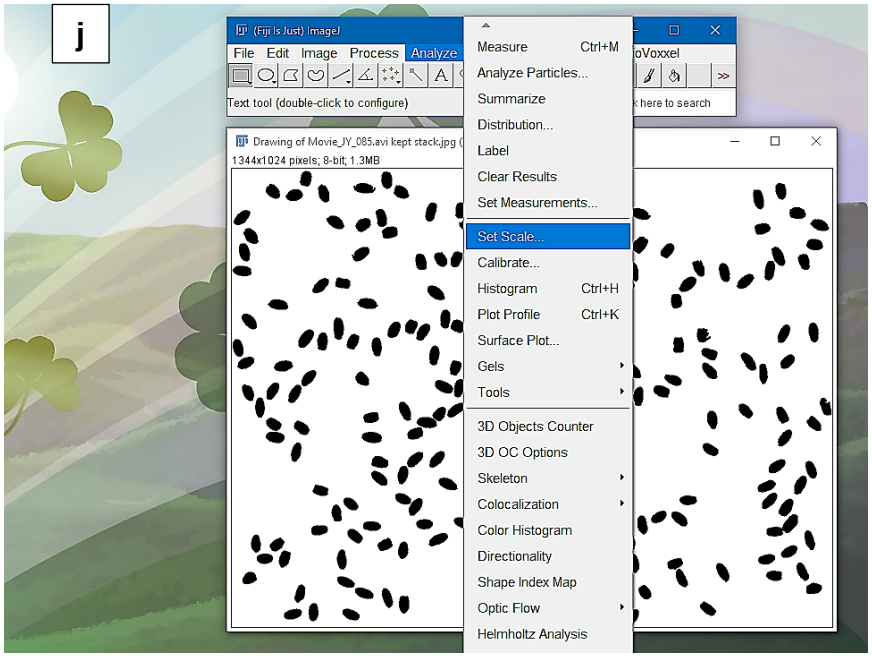
j
(Fiji Is Just) ImageJ
File Edit Image Process Analyze
Text tool (double-click to configure)
Drawing of Movie_JY_085.avi kept stack.jpg
1344x1024 pixels; 8-bit; 1.3MB
Measure Ctrl+M
Analyze Particles...
Summarize
Distribution...
Label
Clear Results
Set Measurements...
Set Scale...
Calibrate...
Histogram Ctrl+H
Plot Profile Ctrl+K
Surface Plot...
Gels
Tools
3D Objects Counter
3D OC Options
Skeleton
Colocalization
Color Histogram
Directionality
Shape Index Map
Optic Flow
Helmholtz Analysis

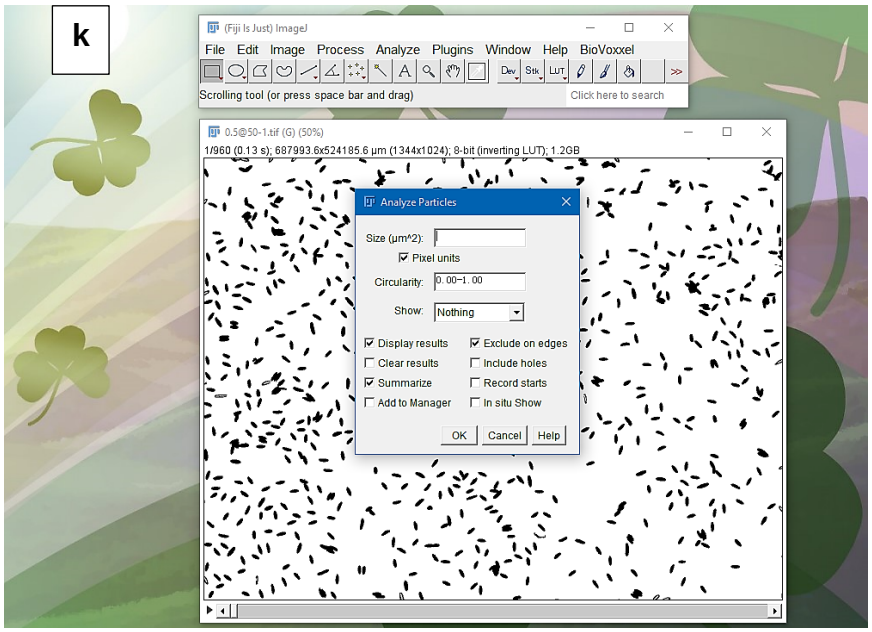
k
(Fiji Is Just) ImageJ
File Edit Image Process Analyze Plugins Window Help BioVoxxel
Scrolling tool (or press space bar and drag)
Click here to search
0.5@50-1.tif (G) (50%)
1/960 (0.13 s); 687993.6x524185.6 µm (1344x1024); 8-bit (inverting LUT); 1.2GB
Analyze Particles
Size (µm^2):
Pixel units
Circularity: 0.00-1.00
Show: Nothing
Display results
Exclude on edges
Clear results
Include holes
Summarize
Record starts
Add to Manager
In situ Show
OK
Cancel
Help

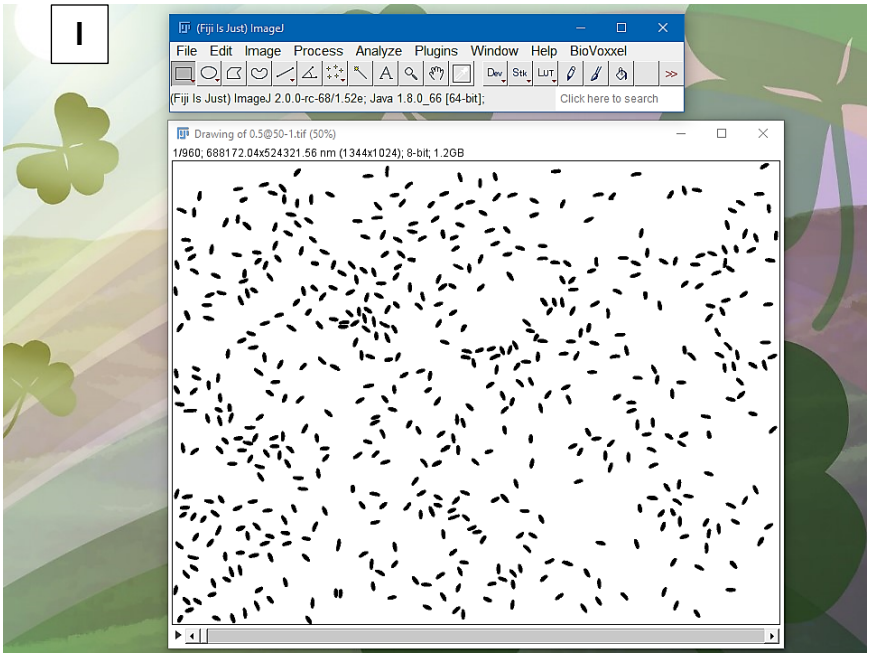

Figure 3.6 (a – l): Image processing for the ellipsoidal particles. Figure a – e, convert video into binary; Figure f – j, characterization within ImageJ; Figure k and l, set the boundary to screen out non-singlet objects for video analysis.

CHAPTER IV

RESULTS AND DISCUSSION

4.1 Introduction

This chapter contains the discussion of acquired data and results from our experiments. To start with, the characterizations of particles were done within ImageJ to confirm the particles possess significantly different geomatical property. From the first series of videos, the phase diagrams were plotted to show conditions (potential difference, frequency) at which colloidal particles have their own status. In addition, how the potential difference and frequency of external electric field, as well as the geometrical property of particles, affect the coagulation kinetics of particles was discussed through the data that we extracted from the other set of videos.

4.2 Colloidal ellipsoids characterization

Figure 4.1 shows the optical micrographs of ellipsoids prepared via the route described above. For an ellipsoid, the aspect ratio equals the ratio of the major axis through the center to the minor axis through the center. Hence, when an ellipsoid possesses an

aspect ratio of 1:1, it is considered as a sphere. In our experiments, we have spherical particles, ellipsoids with low aspect ratio and ellipsoids with high aspect ratio. All particles have a volume equivalent to that of a sphere with a radius of 6 mm. “Low aspect ratio” ellipsoids have an aspect ratio equal to 1.74 ± 0.26, while “high aspect ratio” ellipsoids have an aspect ratio equal to 2.57 ± 0.57. Also, fabrication of ellipsoids does not necessarily produce particles with monodisperse aspect ratios, which indicates a variety of factors may result in broadening of the distribution of aspect ratios produced in a single film. Specifically, two such factors are (1) processing parts of the film that have not stretched uniformly and (2) obtaining particles that were near the interface of the film. The first factor was tried to avoid as much as possible by carefully choosing portions of the film that stretched similarly to each other. Meanwhile, the second factor is hard to avoid, but likely only impacts a small fraction of our particles because comparing with the thickness of a dried film, the diameter of particles is way much smaller. Most particles reside in the volume of the film, rather than near the interface. Additional factors may induce variations in surface chemistry.

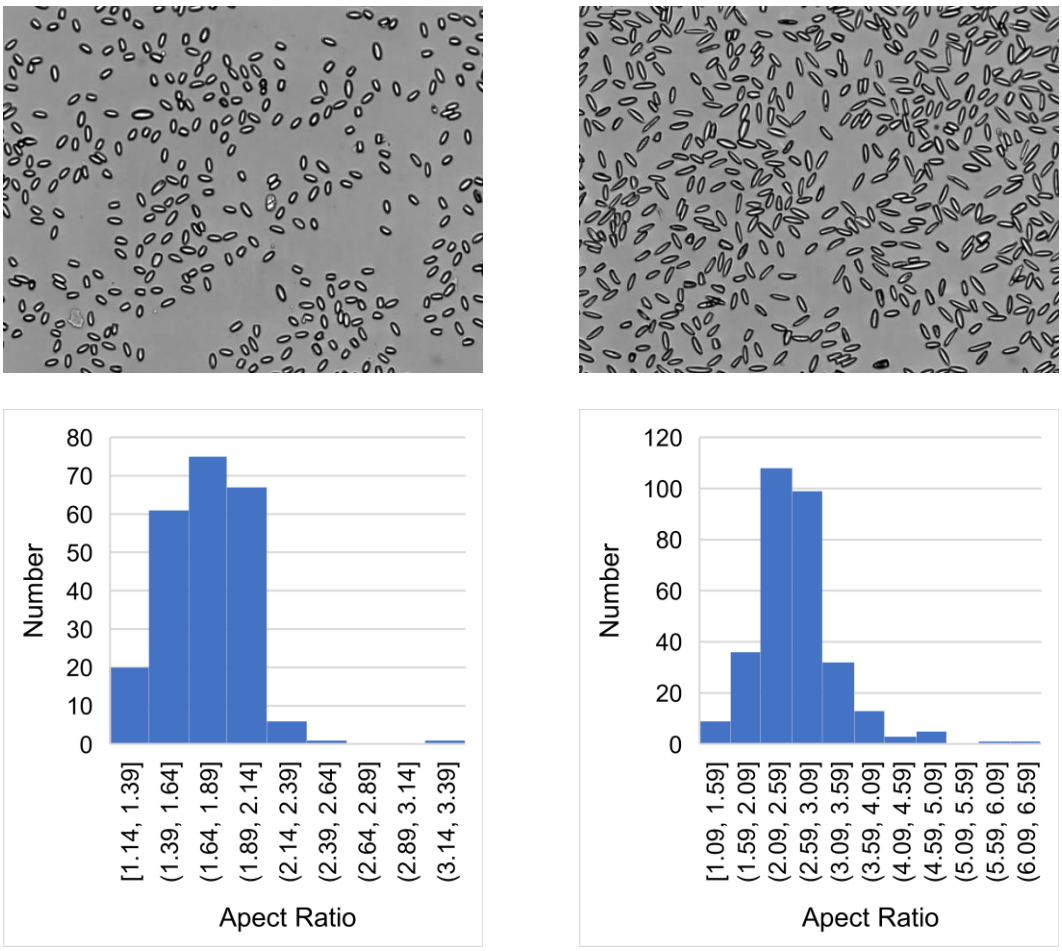

Figure 4.1: Pictures of colloidal ellipsoids under a microscope and histograms of the aspect ratio distribution. Low aspect ratio ellipsoids (left, AR = 1.74 ± 0.26) and high aspect ratio ellipsoid (right, AR = 2.57 ± 0.57).

For instance, adsorption of polyvinyl alcohol chains to the surface of the particle and distributions/migration of bound surface charge as a consequence of stretching may lead to ellipsoids with surface chemistry that varies across the surface of the particle.[16] As noted above, the particles were washed thoroughly in an effort to remove polyvinyl alcohol, but there is little recourse to avoiding variations in surface chemistry from stretching. Note that the later effect has yet to be directly verified in experiments. Other ongoing work in our laboratory seeks to verify that the surface chemistry does vary on a stretched ellipsoid as a consequence of stretching. Additionally, to ensure the surface chemistry of different

colloidal particles is similar, spheres that have involved were obtained from the PVA film as well.

4.3 Cluster formation and destruction in response to an AC electric field

Cluster formation and dissolution were tracked for spheroids of varying aspect ratio in response to an electric field of varying strength and frequency. Initially, spheres with aspect ratio = 1 were manipulated under the external AC electric field by adjusting the electric field parameters, such as the electric field intensity and the frequency. Each video was taken with a fixed electric potential with a frequency that varied every 4 minutes. Each frame of the video was analyzed by finding the average cluster size. The average size equals the total area of particles divided by the number of objects in the visual field. Note that as an internal check, the total area of all objects was also tracked. Regardless of any aggregations or separations happen among particles, the total area of particles in different frames barely change over time, which means when aggregation occurs, particles tend to form a cluster, and this would result in a decrease of objects number and the average size would increase correspondingly. The ratio of dynamic average size to the initial average size indicates the phase of colloidal particles.

Time/min	0	4	8	12	16	20	24	28
Frequency/Hz	0	30	50	100	200	500	1000	3000

Time/min	32	36	40	44	48	52	56
Frequency/Hz	1000	500	200	100	50	30	0

Table 4.1: Starting time points for different applied frequencies.

The table above lists the way of regulating the applied frequency, which can be used for relating the status of particles to the corresponding experimental conditions and that is the strategy for developing the phase diagram.

Spherical colloids experienced regions of either aggregation or separation over the frequency range sampled at fixed electric field intensity (see **Figure 4.2**). Increasing (decreasing) average cluster size is indicated by a region with a positive (negative) slope, showing aggregation (separation) (see **Figure 4.3**). While the sign of the slope indicates the sign of the force, the value of the slope is a result of the strength of the force and the current state of the system. This aggregation behavior is consistent with previous work[12], with aggregation occurring at relatively low frequencies and the critical frequency for them to become repulsive to each other is around 200 Hz. The intensity of aggregation scaled with the electric field strength. Stronger electric fields induced a slope with larger magnitude at aggregating conditions, while there was not a strong dependence on separation of the electric field. Finally, note from **Figure 4.3** the asymmetry of the ensemble behavior for aggregating conditions. Frequency was increased from zero to a peak value (3000 Hz) at 28 minutes, then the applied frequency was reversed. Particles that had been separated remained separated until the aggregating conditions were reached at approximately 44 minutes.

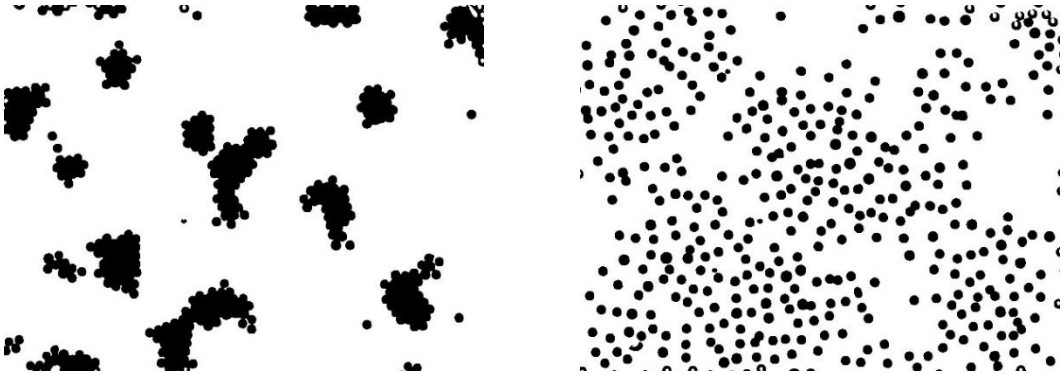

Figure 4.2: The proceed images for estimating the average size of colloidal spheres clusters. Attractive status (left) and repulsive status (right).

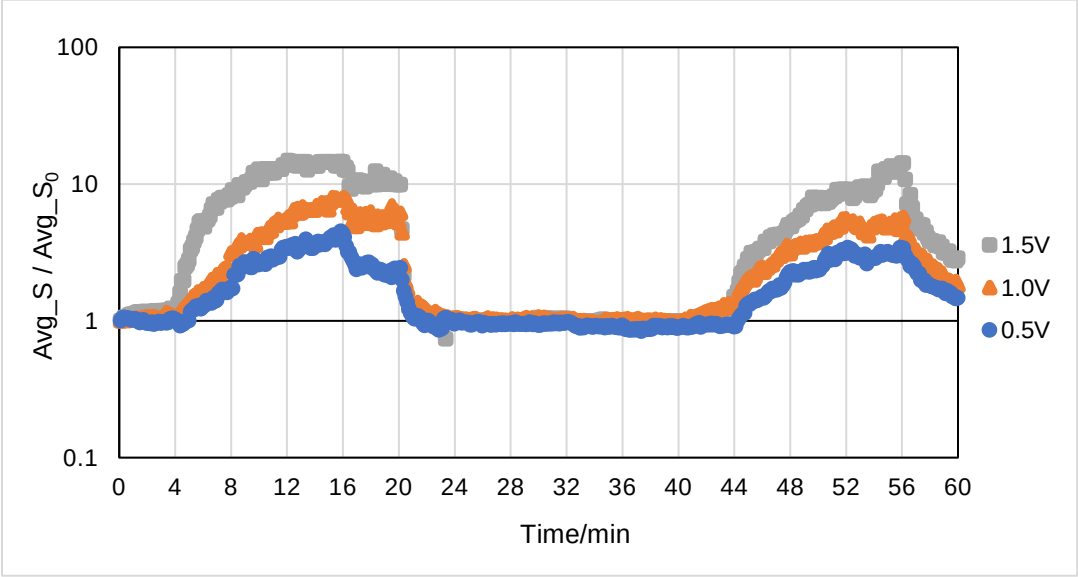

Figure 4.3: Scaled average size of standalone clusters for spherical particles as a function of time for different applied voltages. Squares, 1.5 V; triangles, 1.0 V; circles, 0.5 V.

Data summarized in **Figure 4.3** can be used to formulate a phase diagram (see **Figure 4.4**). The main features of the phase diagram for spheres are the presence of a critical frequency ~200 Hz for all electric field strengths. Particles are attractive from 30 Hz – 100 Hz, but repulsive from 200 Hz – 3000 Hz. Note, that the process is not perfectly reversible, as shown in the phase diagram of increasing frequency and decreasing frequency (see **Figure 4.4**).

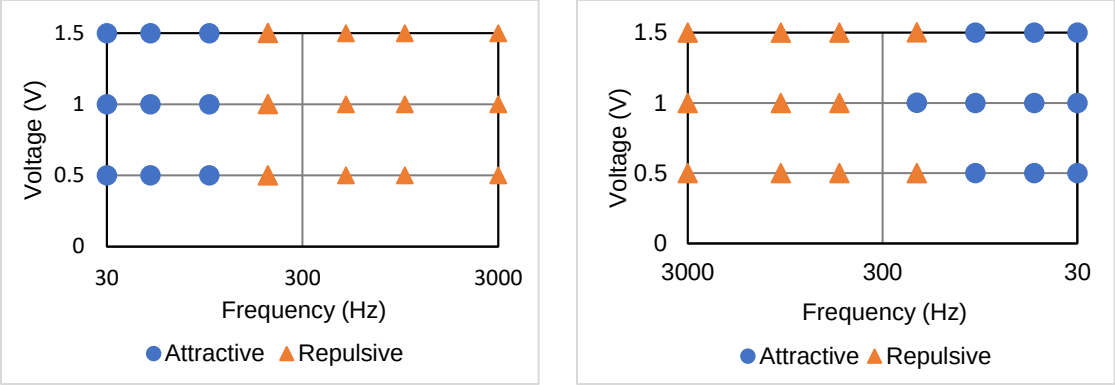

Figure 4.4: Phase Diagram of Spheres for increasing frequency (30 Hz to 3000 Hz) and decreasing frequency (3000 Hz to 30 Hz).

For 200 Hz, the phase diagram of increasing frequency indicates that colloidal spheres remain at the aggregation status, but the phase diagram of decreasing frequency suggests otherwise. Here, we consider the interaction between particles is significantly weakened and have less preference, which makes particles tend to keep their previous states. Since 200 Hz was applied between 100 Hz and 500 Hz in both phase diagram, and the status of colloidal spheres at 100 Hz and 500 Hz were opposite, it is safe to say 200 Hz is in a transition region that resultant interaction starts to change direction. Also, the phase diagrams agree with what Hernández-Navarro, S. *et al.* [32] reported in 2012.

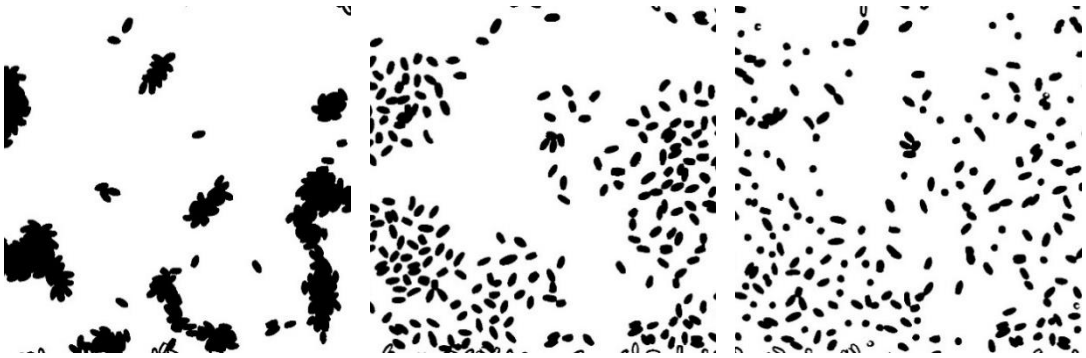

Figure 4.5: The proceed images for estimating the average size of low aspect ratio ellipsoids clusters. Attractive status (left), repulsive status (middle), the repulsive status including standing particles (left).

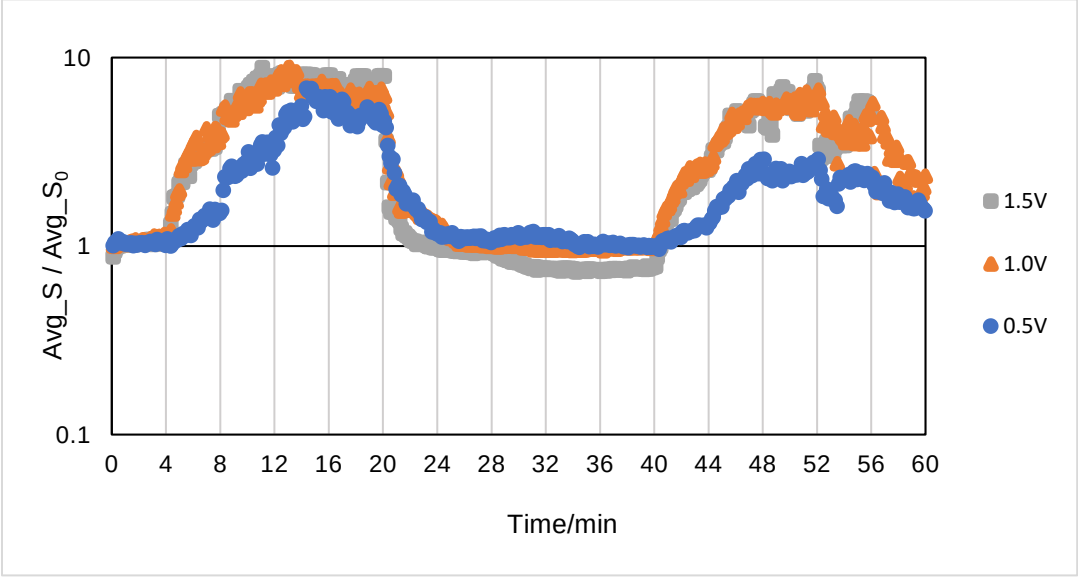

Figure 4.6: Scaled average size of standalone clusters for ellipsoids with low aspect ratio as a function of time for different applied voltages. Squares, 1.5 V; triangles, 1.0 V; circles, 0.5 V.

Low aspect ratio (LAR) ellipsoids displayed behavior similar to that of spheres. LAR ellipsoids rapidly aggregated at low frequency, reached a critical frequency ~200 Hz, and then began to separate at frequencies between 200 Hz – 3000 Hz. One feature that was unique to LAR ellipsoids was the reorientation at certain frequencies. Evidence of ellipsoids reorienting such that the long axis was perpendicular to the electrode (standing

ellipsoid) was first seen in the average cluster size measurement (see **Figure 4.6**). Standing is apparent when the scaled average cluster size decreased below a value of at times between 28 min – 40 min (see **Figure 4.6**). Due to the decreases of the ellipsoid projected area when standing occurs, the scaled area would decrease. All behaviors were summarized in a phase diagram (see **Figure 4.7**).

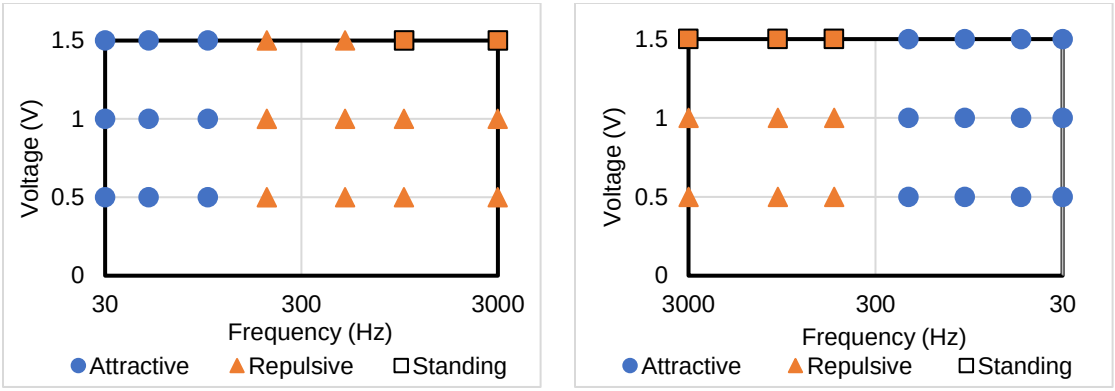

Figure 4.7: Phase diagram of colloidal ellipsoids with low aspect ratio for increasing frequency (30 Hz to 3000 Hz) and decreasing frequency (3000 Hz to 30 Hz).

The phase diagram in **Figure 4.7** for LAR ellipsoids shows a hysteresis in behavior for standing ellipsoids. When ramping frequency, ellipsoids begin to stand at a frequency of ~1000 Hz but remain standing when ramping down frequencies until ~500 Hz. This novel behavior may be a consequence of rotational diffusion relaxation. Ellipsoid standing occurs because the electric field intensity is high enough to force ellipsoid's dipole moment to align with it. When ramping, the dipole torque necessary for alignment must work against the gravitational torque inducing the most probable orientation of lying flat on the electrode surface. When ramping down in frequency, the ellipsoid is already aligned such that a weaker dipole torque is able to sustain that induced alignment, until rotational diffusion causes the ellipsoid to reorient such that the long axis is parallel to the electrode surface.

The reversal frequency (200 Hz) identified from the phase diagram of colloidal spheres is not equivalent to that found for LAR ellipsoids. **Figure 4.7** showed LAR ellipsoids would have another kind of hysteretic behavior at 200 Hz, which is dependent on their previous status and we believe the transition frequency for LAR ellipsoids is around 200 Hz. Also, comparing with spheres, LAR ellipsoids would require a relatively higher frequency to initialize the separation.

The high aspect ratio (HAR) ellipsoids in **Figure 4.8** demonstrated aggregating and separating behavior similar to that of spheres and LAR ellipsoids. HAR ellipsoids aggregated for all electric field strengths up to a critical frequency of ~200 Hz and separated for frequencies between 200 Hz – 3000 Hz (see **Figure 4.9**). The primary difference between LAR and HAR ellipsoids was the duration of relaxation from standing to laying when ramping down the frequency. When ramping up, HAR ellipsoids again stood at a frequency ~1000 Hz but remain standing until the frequency is ramped down to 100 Hz (see **Figure 4.10**). This supports the hypothesis that the hysteresis is a consequence of a rotational diffusion relaxation process. A higher aspect ratio ellipsoid will have a longer relaxation time, thereby requiring a proportionally weaker dipolar force. However, note that the dipolar force may be stronger for a HAR ellipsoid as compared to a LAR ellipsoid at identical electric field conditions. Thus, the difference in hysteresis may be a consequence of both effects. Finally, similar to LAR ellipsoids, around 200 Hz, previously applied frequency would determine if HAR ellipsoids are going to aggregate or separate. It is safe to say that around 200 Hz, the resulting interaction between particles is relatively weaker.

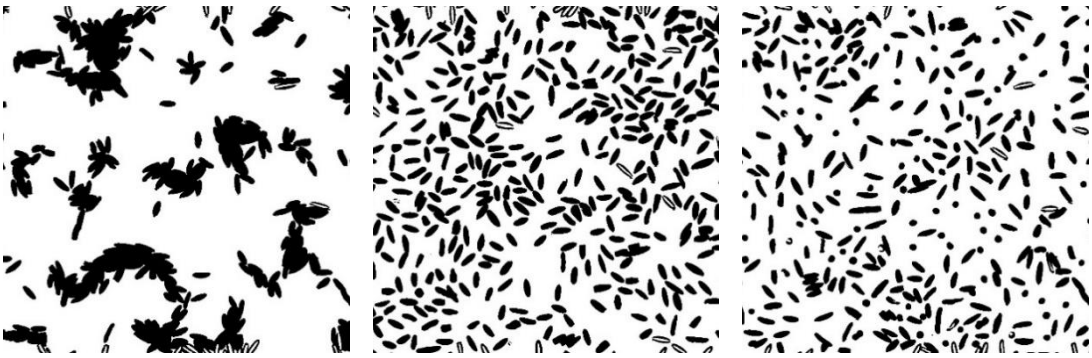

Figure 4.8: The proceed images for estimating the average size of high aspect ratio ellipsoids clusters. Attractive status (left), repulsive status (middle), the repulsive status including standing particles (left).

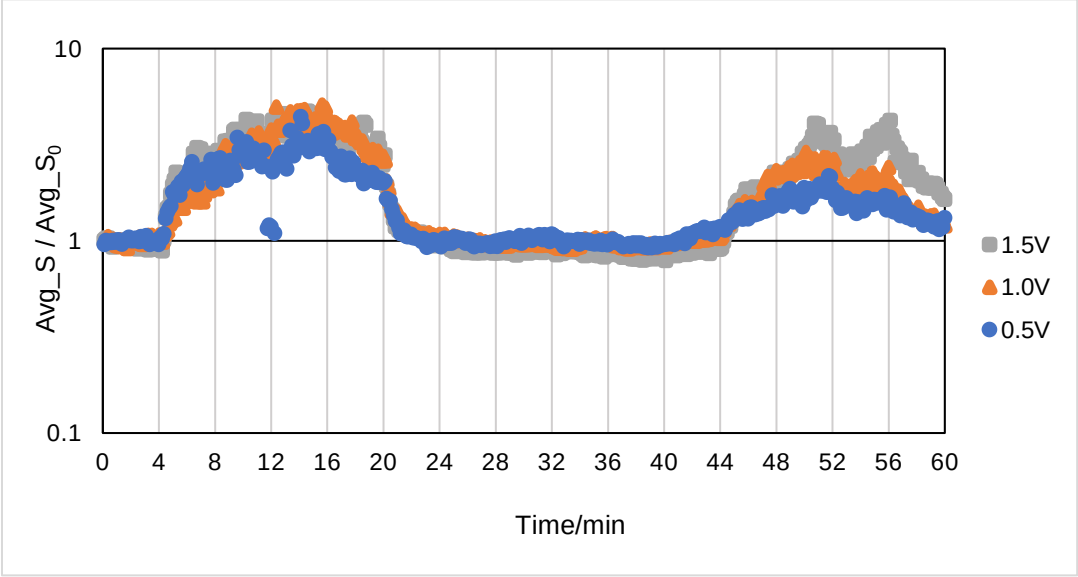

Figure 4.9: Scaled average size of standalone clusters for ellipsoids with high aspect ratio as a function of time for different applied voltages. Squares, 1.5 V; triangles, 1.0 V; circles, 0.5 V.

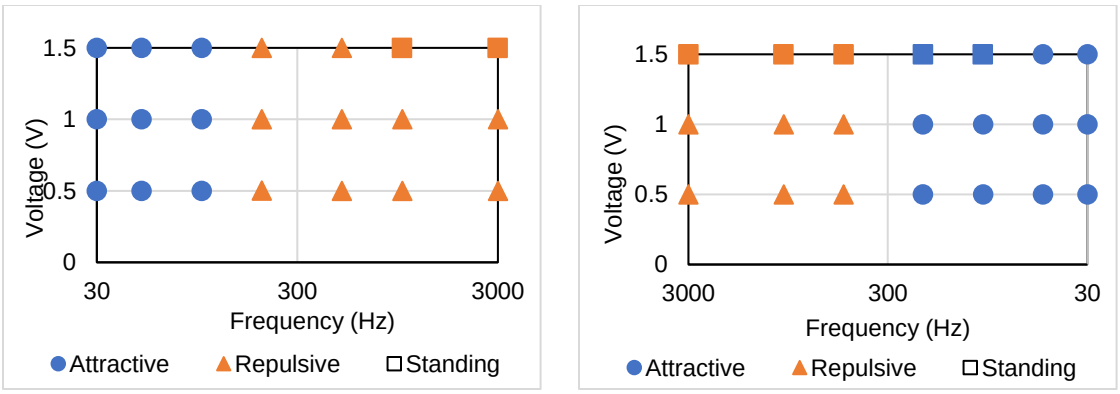

Figure 4.10: Phase diagram of ellipsoids with high aspect ratio for increasing frequency (30 Hz to 3000 Hz) and decreasing frequency (3000 Hz to 30 Hz).

For colloidal ellipsoids, the mean-square angular deviation in time t for the rotational diffusion about the short axis equals to:

$$\langle \theta^2 \rangle = 2D_r t \tag{8}$$

where $\langle \theta^2 \rangle$ is the mean-square angular deviation, D_r is the rotational diffusion coefficient, and t is a given time period.

Since a complete process of the relaxation is forcing a standing ellipsoid (low probability orientation) to lie down (higher probability orientation), the angle of rotation would be fixed at 90° and result in a constant value for the mean-square angular deviations under all circumstances. The inversely proportional relationship between the rotational diffusion coefficient and time demonstrates that ellipsoids possess a higher rotational diffusion coefficient would take a shorter time to relax, which agrees with the rotational diffusion coefficient value in theory. (see **Table 4.2**, values were calculated by the method described in **Section 2.2.4**)

Aspect Ratio	The rotational diffusion coefficient of ellipsoid about a short axis (1/ms)
1.74	3.27×10^{-3}
2.38	2.05×10^{-3}

Table 4.2: Theoretical rotational diffusion coefficient of ellipsoids.

4.4 Determining the rate constant for colloidal aggregation

Data summarized above provided a semi-quantitative description of the response of spheroids with varying aspect ratio to a nearby polarized electrode. We obtained a quantitative description of the aggregation process by treating it with the framework of a chemical reaction and assigned a rate constant of singlet lost (see **Section 2.2.3** for the description). This treatment was previously used for spheres; we repeat similar measurements with spheres and extend the measurements to ellipsoids. Our primary motivation is to determine the impact of aspect ratio on the rate constant for aggregation in response to an AC electric field.

Initially, the rate constant for spheres was measured at a varying electric field. The rate of singlet loss was measured for short time periods. The scaled concentration is equal to the left-hand side of **Equation 4** and it versus time would give an approximate straight-line with slope equal to the rate constant. **Figures 4.11–4.16** show data for the evolution of singlets as a function of time for varying frequency at fixed electrode polarization. Experimental conditions (20 Hz, 30 Hz, 50 Hz, 100 Hz, 200 Hz) were chosen to focus on aggregation only. A strong aggregation process is characterized by a linear relationship

between singlet loss and time with a large magnitude slope, which was handled by a MATLAB Program (see **Appendix 2**).

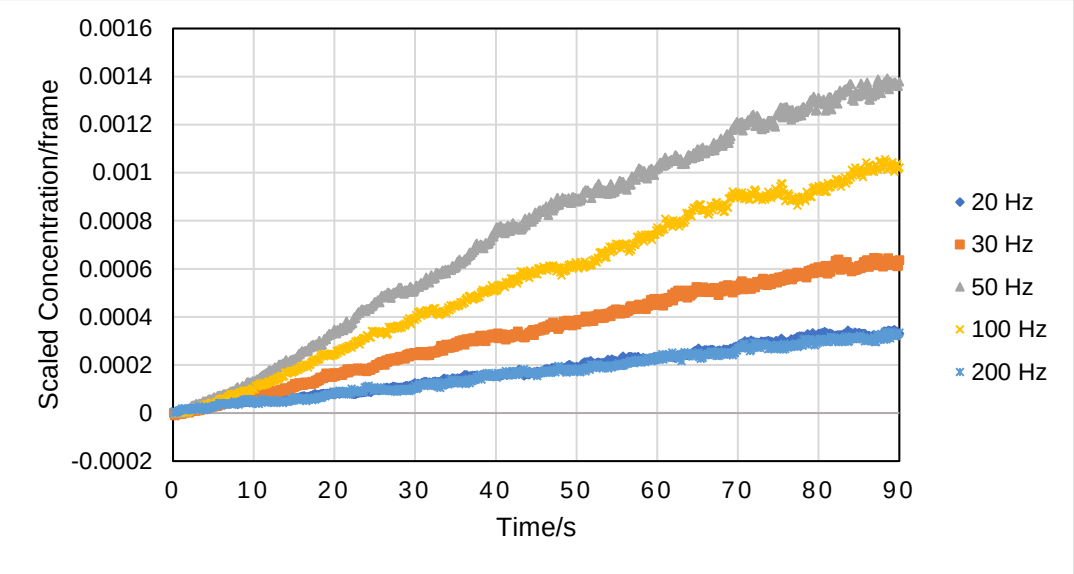

Figure 4.11: The scaled concentration slopes for colloidal spheres at 1.0 V.

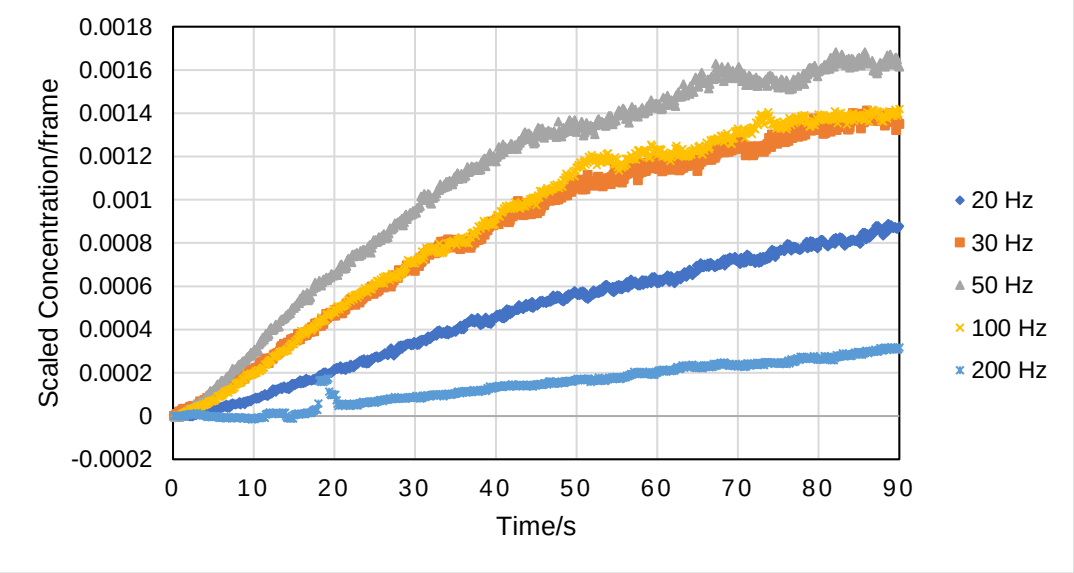

Figure 4.12: The scaled concentration slopes for colloidal spheres at 1.5 V.

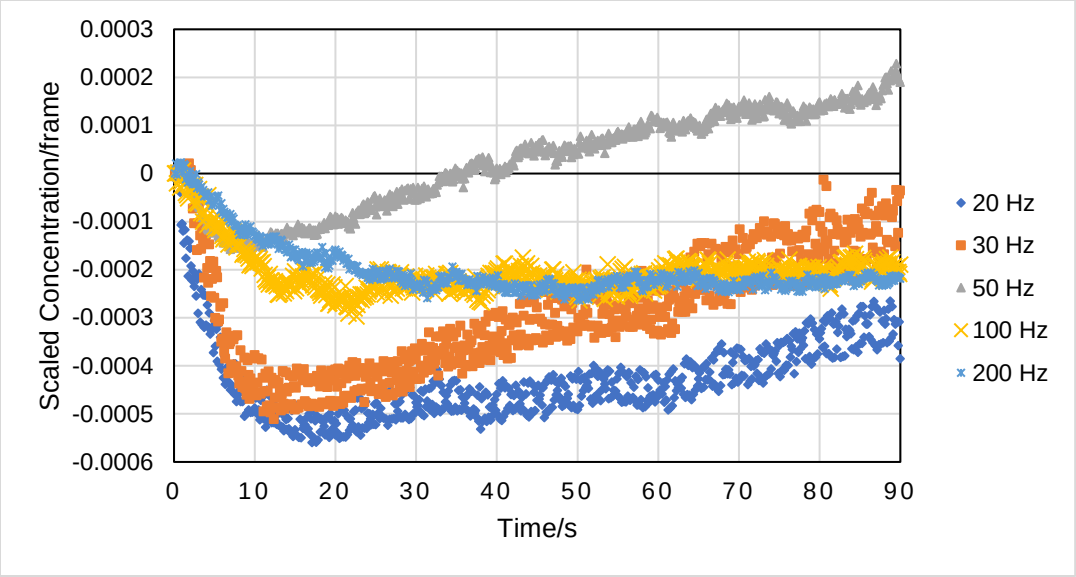

Figure 4.13: The scaled concentration slopes for LAR ellipsoids at 1.0 V.

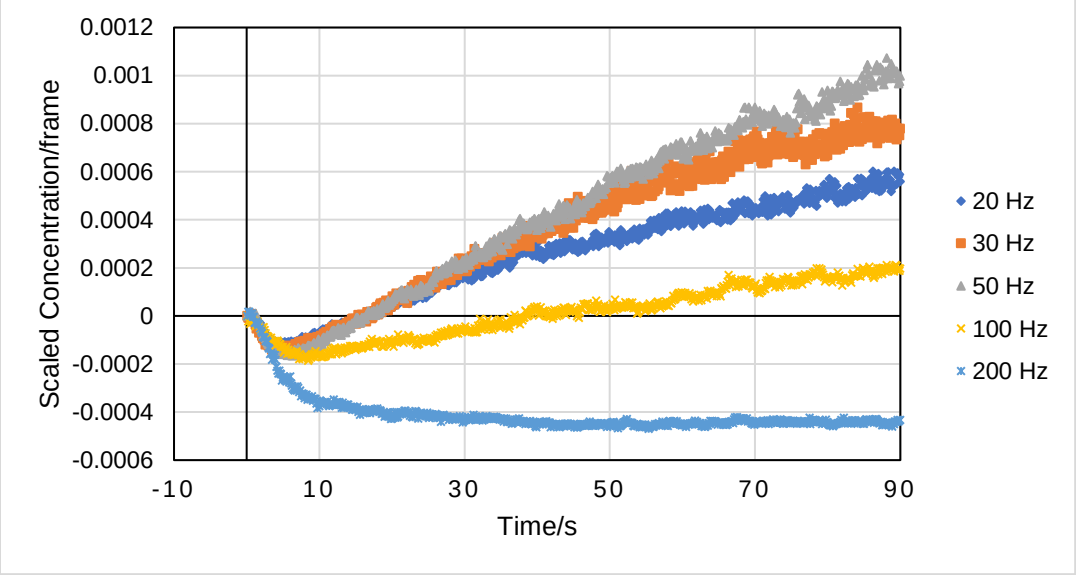

Figure 4.14: The scaled concentration slopes for LAR ellipsoids at 1.5 V.

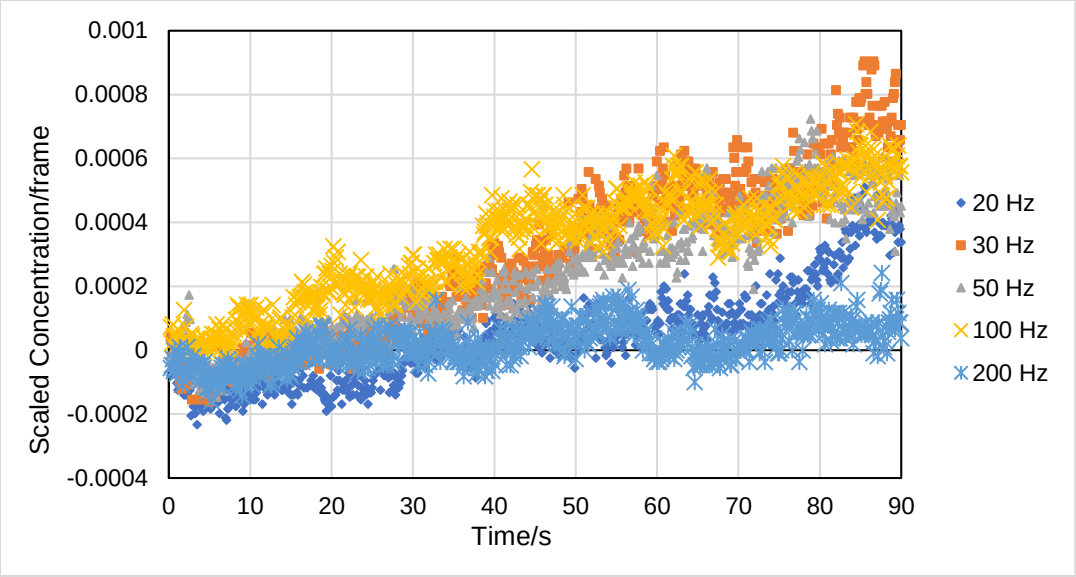

Figure 4.15: The scaled concentration slopes for HAR ellipsoids at 1.0 V.

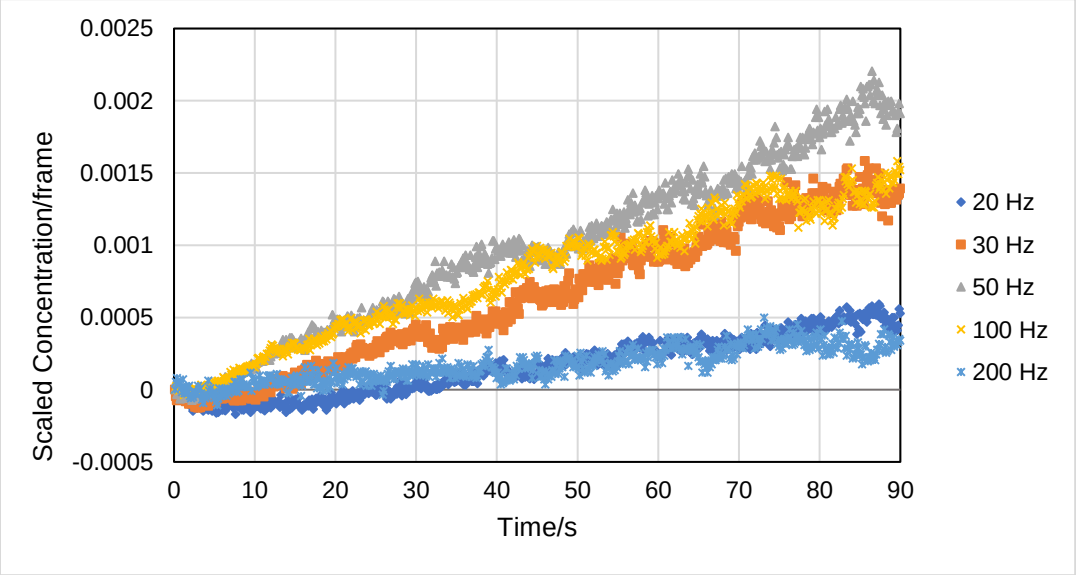

Figure 4.16: The scaled concentration slopes for HAR ellipsoids at 1.5 V.

The value for these slopes was summarized (see **Table 4.3**, **4.4**, and **4.5**) and plotted as a function of frequency for fixed polarization (see **Figure 4.17–4.21**). As shown in **Figure 4.17–4.19**, the higher applied voltage would result in a higher rate constant. In addition, the rate constant increases with the growing frequency until it reaches a maximum

value and then decreased as frequency keep growing. This tendency is applicable to all three types of colloidal particles and the frequency at which rate constant has a maximum value is targeted as m-frequency (f_m). As the peaks always appear at 50 Hz, the aspect ratio of colloidal particles would not impact the f_m.

The critical frequency (f_c) that discussed in **Section 4.3** characterizes the reversal of the resulting interaction and the phase diagram indicated f_c of LAR ellipsoids is differ from spheres and HAR ellipsoids, which could also be identified by **Figure 4.20**, **4.21**. Ramping up the applied frequency from 100 Hz to 200 Hz, the rate constants for all three kinds of particles are significantly dropped, but spheres and HAR ellipsoids still preserve a positive value, which suggests that LAR ellipsoids have started to separate from each other already. This could also be related to the hysteresis that we have observed from spheres and HAR ellipsoids (see **Figure 4.4**, **4.10**).

Furthermore, both LAR and HAR ellipsoids behaved in a fashion similar to that of the spheres in response to the electric field, but the value of the rate constants was systematically different from those of spheres. Spheres tend to have the highest rate constant among them. From the standpoint of taking account of the aspect ratio for spheres (=1), assuming colloidal ellipsoids have a relatively lower aspect ratio would behave more like spheres it's more reasonable, but the compared results for different particles suggested otherwise (see **Figure 4.20** and **4.21**). The rate constant for HAR ellipsoids is generally closer to spheres, which means, in term of the assembling rate, the geometric property of HAR contribute to the aggregation by altering the streamline around colloidal ellipsoids in a more favorable way.

P\ *f*	20 Hz	30 Hz	50 Hz	100 Hz	200 Hz
1.0 V	3.549×10^{-6}	8.438×10^{-6}	1.906×10^{-5}	1.389×10^{-5}	3.263×10^{-6}
1.5 V	1.196×10^{-5}	2.410×10^{-5}	3.364×10^{-5}	2.575×10^{-5}	3.775×10^{-6}

Table 4.3: Value of rate constant of spheres aggregation for varying frequency at a fixed potential.

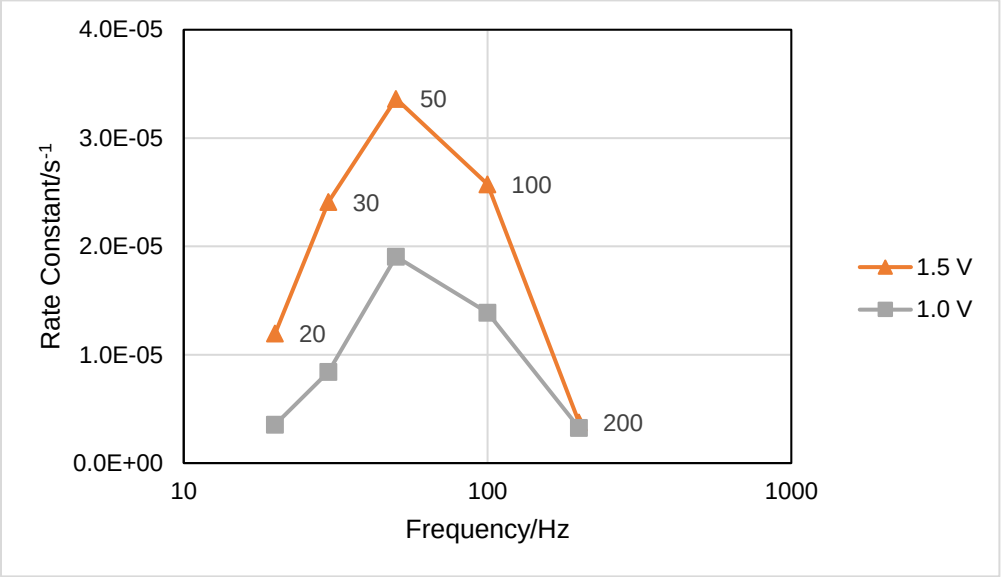

Figure 4.17: Rate constant of spheres aggregation for varying frequency at a fixed potential.

P\ *f*	20 Hz	30 Hz	50 Hz	100 Hz	200 Hz
1.0 V	1.741×10^{-6}	4.565×10^{-6}	5.417×10^{-6}	1.115×10^{-6}	0
1.5 V	1.007×10^{-5}	1.422×10^{-5}	1.607×10^{-5}	5.360×10^{-6}	0

Table 4.4: Value of rate constant of LAR ellipsoids aggregation for varying frequency at a fixed potential.

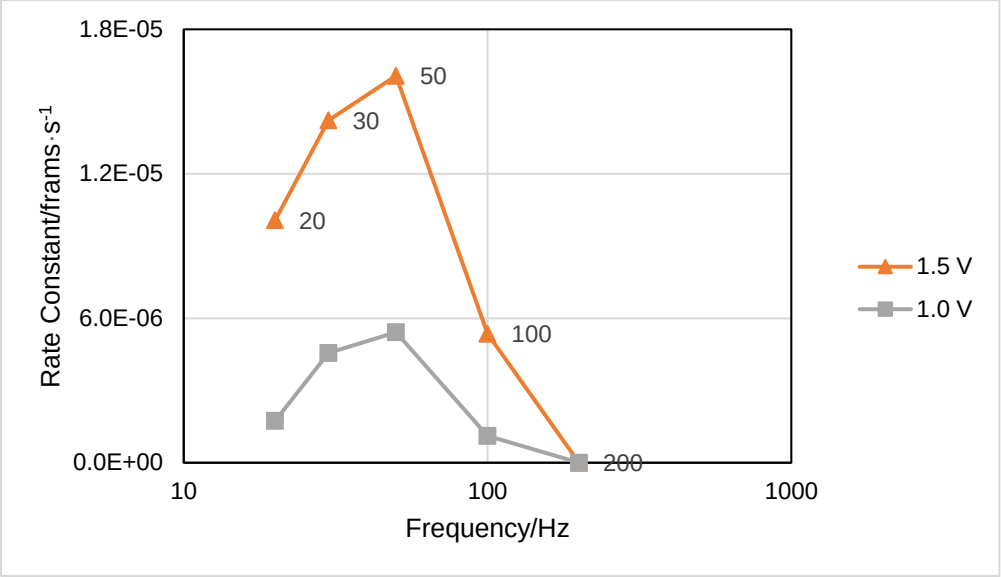

Figure 4.18: Rate constant of LAR ellipsoids aggregation for varying frequency at a fixed potential.

P\ *f*	20 Hz	30 Hz	50 Hz	100 Hz	200 Hz
1.0 V	4.358×10^{-6}	6.198×10^{-6}	8.837×10^{-6}	7.994×10^{-6}	2.620×10^{-6}
1.5 V	8.291×10^{-6}	1.748×10^{-5}	2.503×10^{-5}	2.123×10^{-5}	4.595×10^{-6}

Table 4.5: Value of rate constant of HAR ellipsoids aggregation for varying frequency at a fixed potential.

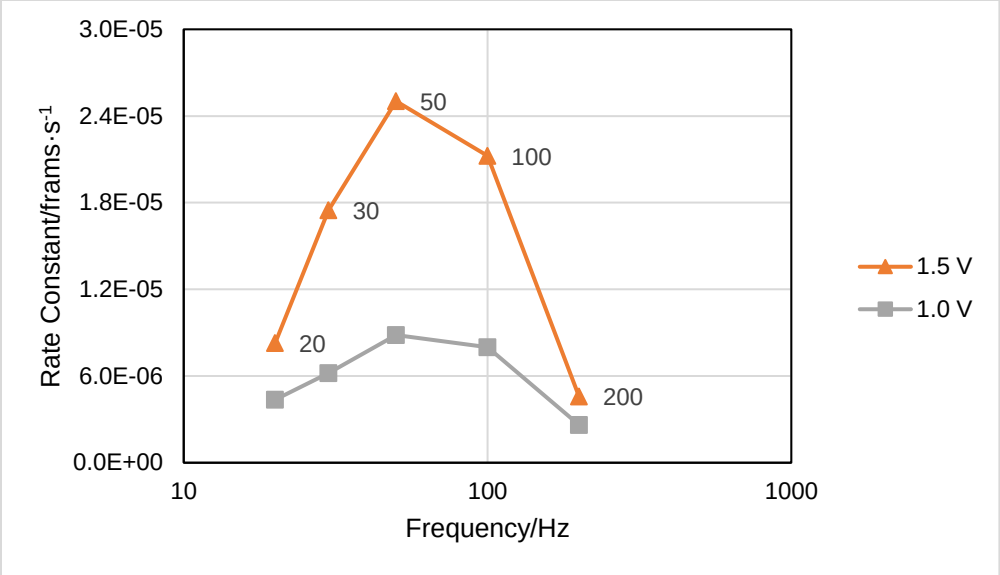

Figure 4.19: Rate constant of HAR ellipsoids aggregation for varying frequency at a fixed potential.

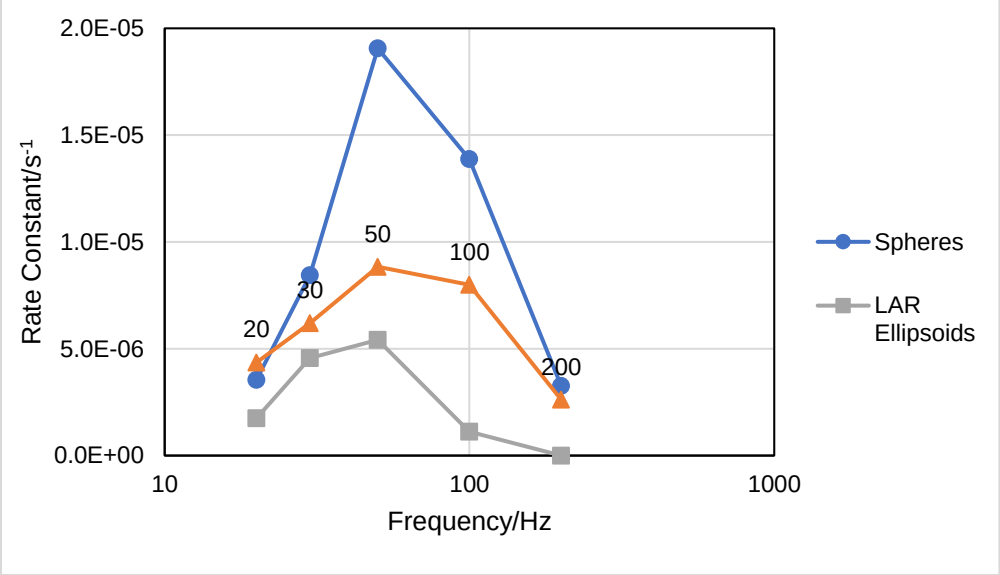

Figure 4.20: Rate constant of aggregation for varying frequency at 1.0 V.

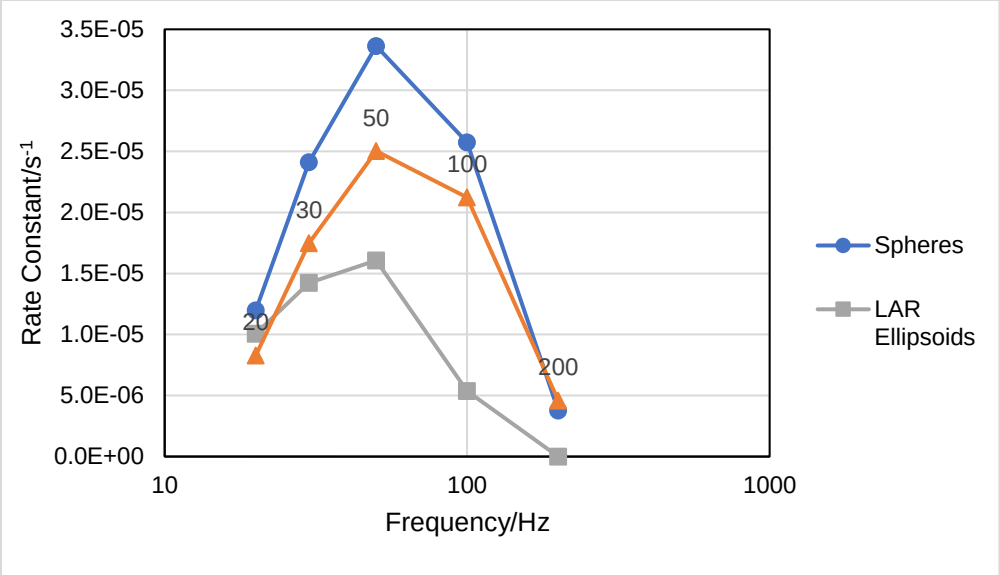

Figure 4.21: Rate constant of aggregation for varying frequency at 1.0 V.

CHAPTER V

CONCLUSIONS AND RECOMMENDATIONS

5.1 Conclusions

In our experiments, we determined the phase diagrams for colloidal spheres, LAR ellipsoids, and HAR ellipsoids, which could be used to identify the response of colloidal ellipsoids near a polarized electrode. The most surprising result was the existence of hysteretic responses of standing ellipsoids' relaxation, which represents the aspect ratio of ellipsoids will significantly affect the motion of ellipsoids under an AC electric field. Also, the critical frequency for interaction reversal is around 200 Hz. Different aspect ratios would result in dissimilar phase diagrams and rate constants. Moreover, the rate constant for the rapid aggregation was obtained and plotted, from which a positive value indicates aggregation and that agreed with both the phase diagram and what we have observed. For all assembly of particles, a higher potential tends to bring about a greater rate constant. Besides, in all plots, the maximum rate constant always locates at 50 Hz regardless of the different aspect ratio of colloidal particles. However, under the same potential, the magnitudes of them are not alike. Specifically, LAR ellipsoids possess the lowest magnitude among them. In another word, rate constant results are parallel to the fact we

mentioned above that colloidal spheres and HAR ellipsoids tend to share similar responses under an AC electric field when comparing with LAR ellipsoids.

5.2 Recommendations

As mentioned in Section 4.3, the relaxation time could be potentially impacted by both the dipolar force and the geometric difference. For a further verification, we could isolate the effect of the geometric difference and study it individually via applying a suitable condition (such as 3.0 V at 1000 Hz) under which the long axis of colloidal ellipsoids would be aligned with the electric field and withdraw that external electric field after most of the ellipsoids in the visual field are in standing status. Without the introduced external force, the gravity would change the “standing up” statue of ellipsoids into “lying down” over time and by taking videos of this relaxation process, we would be able to explore the relationship between the aspect ratio of colloidal ellipsoids and the length of relaxation time. Moreover, another series of rod-like ellipsoids and more different fixed polarizations for the determination of rate constant would be brought in for the future experiments, so that we could systematically study more about the kinetics of aggregation.

REFERENCES

1. Lattuada, M., & Hatton, T. A. (2011). Synthesis, properties, and applications of Janus nanoparticles. Nano Today, 6(3), 286-308.
2. Glotzer, S. C., & Solomon, M. J. (2007). Anisotropy of building blocks and their assembly into complex structures. *Nature materials*, *6*(8), 557.
3. Du, J., & O'Reilly, R. K. (2011). Anisotropic particles with patchy, multicompartment and Janus architectures: preparation and application. Chemical Society Reviews, 40(5), 2402-2416.
4. Chen, C. H., Shah, R. K., Abate, A. R., & Weitz, D. A. (2009). Janus particles templated from double emulsion droplets generated using microfluidics. Langmuir, 25(8), 4320-4323.
5. Jiang, S., Chen, Q., Tripathy, M., Luijten, E., Schweizer, K. S., & Granick, S. (2010). Janus particle synthesis and assembly. *Advanced materials*, *22*(10), 1060-1071.
6. McConnell, M. D., Kraeutler, M. J., Yang, S., & Composto, R. J. (2010). Patchy and multiregion janus particles with tunable optical properties. Nano letters, 10(2), 603-609.
7. Nisisako, T., Torii, T., Takahashi, T., & Takizawa, Y. (2006). Synthesis of monodisperse bicolored janus particles with electrical anisotropy using a microfluidic Co‐Flow system. Advanced Materials, 18(9), 1152-1156.
8. Yoshida, M., Roh, K. H., & Lahann, J. (2007). Short-term biocompatibility of biphasic nanocolloids with potential use as anisotropic imaging probes. Biomaterials, 28(15), 2446-2456.

9. Smoukov, S. K., Gangwal, S., Marquez, M., & Velev, O. D. (2009). Reconfigurable responsive structures assembled from magnetic Janus particles. Soft Matter, 5(6), 1285-1292.
10. Du, J., & Armes, S. P. (2010). Patchy multi-compartment micelles are formed by direct dissolution of an ABC triblock copolymer in water. Soft Matter, 6(19), 4851-4857.
11. Heatley, K. L., Ma, F., & Wu, N. (2017). Colloidal molecules assembled from binary spheres under an AC electric field. Soft matter, 13(2), 436-444.
12. Ma, F., Wang, S., Smith, L., & Wu, N. (2012). Two-Dimensional Assembly of Symmetric Colloidal Dimers under Electric Fields. Advanced Functional Materials, 22(20), 4334-4343.
13. Kim, J. W., Larsen, R. J., & Weitz, D. A. (2006). Synthesis of nonspherical colloidal particles with anisotropic properties. Journal of the American Chemical Society, 128(44), 14374-14377.
14. Ho, C. C., Keller, A., Odell, J. A., & Ottewill, R. H. (1993). Preparation of monodisperse ellipsoidal polystyrene particles. Colloid and Polymer Science, 271(5), 469-479.
15. Crassous, J. J., Mihut, A. M., Wernersson, E., Pfleiderer, P., Vermant, J., Linse, P., & Schurtenberger, P. (2014). Field-induced assembly of colloidal ellipsoids into well-defined microtubules. Nature communications, 5, 5516.
16. Madivala, B., Fransaer, J., & Vermant, J. (2009). Self-assembly and rheology of ellipsoidal particles at interfaces. Langmuir, 25(5), 2718-2728.

17. Wirth, C. L., Sides, P. J., & Prieve, D. C. (2013). Electrolyte dependence of particle motion near an electrode during ac polarization. Physical Review E, 87(3), 032302.
18. Reuss, F. F. (1809). Charge-induced flow. Proceedings of the Imperial Society of Naturalists of Moscow, 1809, 3, 327-344.
19. Ma, F., Wu, N. (2016). Electric-field Assembly of Colloids with Anisotropic Interactions
20. Prieve, D. C., Sides, P. J., & Wirth, C. L. (2010). 2-D assembly of colloidal particles on a planar electrode. Current Opinion in Colloid & Interface Science, 15(3), 160-174.
21. Sides, P. J., Wirth, C. L., & Prieve, D. C. (2012). Mechanisms of Directed Assembly of Colloidal Particles in Two Dimensions by Application of Electric Fields. In Electrophoretic Deposition of Nanomaterials (pp. 3-71). Springer, New York, NY.
22. Solomentsev, Y., Böhmer, M., & Anderson, J. L. (1997). Particle clustering and pattern formation during electrophoretic deposition: a hydrodynamic model. Langmuir, 13(23), 6058-6068.
23. Ristenpart, W. D., Aksay, I. A., & Saville, D. A. (2007). Electrohydrodynamic flow around a colloidal particle near an electrode with an oscillating potential. Journal of Fluid Mechanics, 575, 83-109.
24. Ristenpart, W. D., Aksay, I. A., & Saville, D. A. (2004). Assembly of colloidal aggregates by electrohydrodynamic flow: Kinetic experiments and scaling analysis. Physical Review E, 69(2), 021405.

25. Mikkelsen, A., Wojciechowski, J., Rajňák, M., Kurimský, J., Khobaib, K., Kertmen, A., & Rozynek, Z. (2017). Electric field-driven assembly of sulfonated polystyrene microspheres. Materials, 10(4), 329.
26. Zheng, Z., & Han, Y. (2010). Self-diffusion in two-dimensional hard ellipsoid suspensions. The Journal of chemical physics, 133(12), 124509.
27. Han, Y., Alsayed, A. M., Nobili, M., Zhang, J., Lubensky, T. C., & Yodh, A. G. (2006). Brownian motion of an ellipsoid. Science, 314(5799), 626-630.
28. Hernández-Navarro, S., Ignés-Mullol, J., Sagués, F., & Tierno, P. (2012). Role of anisotropy in electrodynamically induced colloidal aggregates. Langmuir, 28(14), 5981-5986.
29. Rallison, J. M., & Harding, S. E. (1985). Excluded volume for pairs of triaxial ellipsoids at dominant Brownian motion. Journal of colloid and interface science, 103(1), 284-289.
30. Kode, V. R. (2016). Production of polystyrene ellipsoidal colloidal particles via film stretching.
31. Gong, J., & Wu, N. (2017). Electric-field assisted assembly of colloidal particles into ordered nonclose-packed arrays. Langmuir, 33(23), 5769-5776.
32. Hernández-Navarro, S., Ignés-Mullol, J., Sagués, F., & Tierno, P. (2012). Role of anisotropy in electrodynamically induced colloidal aggregates. Langmuir, 28(14), 5981-5986.

APPENDIX

1. ImageJ micro code for analyzing videos

```
run("Duplicate...", "duplicate");  % Initialize a processed video for further analysis
setOption("BlackBackground", false); % Choose the light background
run("Make Binary", "method=Default background=Light calculate"); % isolate targeting particles and draw the outlines for them
run("Fill Holes", "stack"); % Make the outline of particles become solid spots
run("Analyze Particles...", "size=100-200 pixel show=[Bare Outlines] display exclude include summarize stack"); % Set the right pixel size range for particles to screen out irrelevant objects and generate data regarding particles/clusters
```

2. MATLAB code for estimating the rate constant of aggregation

```
start_node = 241; % Starting point from the raw data
num_node = 480; % Number of points of one trendline, which represents the chosen time period for the raid aggregation.

num_file = 8; % Number of data files that collected from ImageJ analysis

Pcdata = zeros(num_node, num_file+1); % Build an all-zero matrix to initiate the storage of processed data

Pcdata(:, 1) = 0:0.125:(num_node-1)*0.125; % Define the time series
```

```
for i = 1:num_file

    filename = sprintf('%d.csv', i);
    Seldata = csvread(filename, start_node, 1, [start_node, 1, start_node+num_node-1, 1]);

    Pcdata(:, i+1) = 1./Seldata- 1/Seldata(1,1);

end

% Save the processed data
file_name_save = 'ProcessData.xlsx';
xlswrite(file_name_save,Pcdata)

% Plot the processed data to obtain trendlines
figure(1)
C = {'r.', 'c.', 'b.', 'g.', 'y.', 'm.', 'k.',...
     'r*', 'c*', 'b*', 'g*', 'y*', 'm*', 'k*',...
     'ro', 'co', 'bo', 'go', 'yo', 'mo', 'ko',...
     'r^', 'c^', 'b^', 'g^', 'y^', 'm^', 'k6',...
     'rs', 'cs', 'bs', 'gs', 'ys', 'ms', 'ks',...
     'rx', 'cx', 'bx', 'gx', 'yx', 'mx', 'kx',...
     'r<', 'c<', 'b<', 'g<', 'y<', 'm<', 'k<'};
```

```
for j = 1:num_file
plot(Pcdata(:, 1), Pcdata(:, j+1), C{j})
hold on;
end
hold off;

% Linear regression of trendlines

Rate_Constant = zeros(num_file, 1); % Define dimension of Slope (equals to
Rate_Constant) matrix

for k = 1:num_file
   p =  polyfit(Pcdata(:, 1), Pcdata(:, k+1),1);
   Rate_Constant(k) = p(1);
end

% Save the Rate_Constant
file_name_save_Rate_Constant = 'ProcessData_Rate_Constant.xlsx';
xlswrite(file_name_save_Rate_Constant, Rate_Constant)
```